

**AFRL-SN-WP-TR-2001-1107**

**DEPOSITION AND CHARACTERIZATION  
OF BARRIER METALS**



**KEVIN D. LEEDY**

**AFRL/SNDI, BUILDING 620  
2241 AVIONICS CIRCLE, STE. 20  
WRIGHT-PATTERSON AIR FORCE BASE, OH 45433-7322**

**SEPTEMBER 2001**

**FINAL REPORT FOR PERIOD OF 09 MARCH 1995 – 30 APRIL 2001**

**Approved for public release; distribution unlimited**

**SENSORS DIRECTORATE  
AIR FORCE RESEARCH LABORATORY  
AIR FORCE MATERIEL COMMAND  
WRIGHT-PATTERSON AIR FORCE BASE, OH 45433-7318**

# REPORT DOCUMENTATION PAGE

Form Approved OMB No.  
0704-0188

Public reporting burden for this collection of information is estimated to average 1 hour per response, including the time for reviewing instructions, searching existing data sources, gathering and maintaining the data needed, and completing and reviewing this collection of information. Send comments regarding this burden estimate or any other aspect of this collection of information, including suggestions for reducing this burden to Department of Defense, Washington Headquarters Services, Directorate for Information Operations and Reports (0704-0188), 1215 Jefferson Davis Highway, Suite 1204, Arlington, VA 22202-4302. Respondents should be aware that notwithstanding any other provision of law, no person shall be subject to any penalty for failing to comply with a collection of information if it does not display a currently valid OMB control number. PLEASE DO NOT RETURN YOUR FORM TO THE ABOVE ADDRESS.

|  |                                |   |
|--|--------------------------------|---|
| <b>1. REPORT DATE (DD-MM-YYYY)</b><br>01-09-2001 | <b>2. REPORT TYPE</b><br>Final | <b>3. DATES COVERED (FROM - TO)</b><br>09-03-1995 to 30-04-2001 |
|--|--------------------------------|---|

|   |                                   |
|---|-----------------------------------|
| <b>4. TITLE AND SUBTITLE</b><br>Deposition and Characterization of Barrier Metals<br>Unclassified | <b>5a. CONTRACT NUMBER</b>        |
|   | <b>5b. GRANT NUMBER</b>           |
|   | <b>5c. PROGRAM ELEMENT NUMBER</b> |

|  |                             |
|--|-----------------------------|
| <b>6. AUTHOR(S)</b><br>Leedy, Kevin D. ; | <b>5d. PROJECT NUMBER</b>   |
|  | <b>5e. TASK NUMBER</b>      |
|  | <b>5f. WORK UNIT NUMBER</b> |

|  |   |
|--|---|
| <b>7. PERFORMING ORGANIZATION NAME AND ADDRESS</b><br>AFRL/SNDI, Building 620<br>2241 Avionics Circle, Ste. 20<br>Wright-Patterson AFB, OH45433-7322 | <b>8. PERFORMING ORGANIZATION REPORT NUMBER</b> |
|--|---|

|   |   |
|---|---|
| <b>9. SPONSORING/MONITORING AGENCY NAME AND ADDRESS</b><br>Sensors Directorate<br>Air Force Research Laboratory<br>Air Force Materiel Command<br>Wright-Patterson AFB, OH45433-7318 | <b>10. SPONSOR/MONITOR'S ACRONYM(S)</b>       |
|   | <b>11. SPONSOR/MONITOR'S REPORT NUMBER(S)</b> |

|   |
|---|
| <b>12. DISTRIBUTION/AVAILABILITY STATEMENT</b><br>APUBLIC RELEASE |
|---|

|                                |
|--------------------------------|
| <b>13. SUPPLEMENTARY NOTES</b> |
|--------------------------------|

|  |
|--|
| <b>14. ABSTRACT</b><br>Increasing complexity and shrinking sizes of integrated circuits necessitate the development of new materials and processes to meet current system requirements of high performance and reliability in smaller electronic assemblies. In order to achieve the system performance, materials with incompatible physical and electrical properties are often placed into direct contact with one another. Applications such as area array interconnection of Si devices using lead/tin solders, vias in Si integrated circuits and gold contacts to GaAs circuits require the use of barrier metals to physically and chemically separate materials that would otherwise react and form undesirable by-products or significantly decrease the reliability of the electronic system. This effort was initiated in order to advance the understanding of basic mechanisms and influences of processing on the performance of barrier metals. Deposition of the barrier metals was conducted using physical vapor deposition, unique barrier metal alloys that could not be fabricated by thermodynamic equilibrium methods were developed. Characterization of the processing and materials was performed to better understand the essential mechanisms required for high quality barrier metals. |
|--|

|   |
|---|
| <b>15. SUBJECT TERMS</b><br>Barrier; physical vapor deposition; thin film |
|---|

|  |   |                                  |   |
|--|---|----------------------------------|---|
| <b>16. SECURITY CLASSIFICATION OF:</b> | <b>17. LIMITATION OF ABSTRACT</b><br>Same as Report (SAR) | <b>18. NUMBER OF PAGES</b><br>34 | <b>19. NAME OF RESPONSIBLE PERSON</b><br>Fenster, Lynn<br>lfenster@dtic.mil |
|--|---|----------------------------------|---|

|                           |                             |                              |   |
|---------------------------|-----------------------------|------------------------------|---|
| a. REPORT<br>Unclassified | b. ABSTRACT<br>Unclassified | c. THIS PAGE<br>Unclassified | <b>19b. TELEPHONE NUMBER</b><br>International Area Code<br>Area Code Telephone Number<br>703767-9007<br>DSN<br>427-9007 |
|---------------------------|-----------------------------|------------------------------|---|

## NOTICE

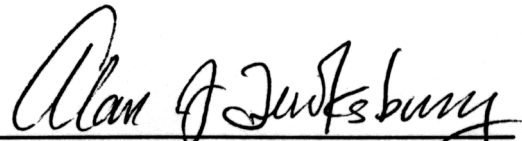
Using government drawings, specifications, or other data included in this document for any purpose other than government procurement does not in any way obligate the U.S. Government. The fact that the government formulated or supplied the drawings, specifications, or other data does not license the holder or any other person or corporation; or convey and rights or permission to manufacture, use, or sell any patented invention that may relate to them.

This report has been reviewed by the Office of Public Affairs (ASC/PA) and is releasable to the National Technical Information Service (NTIS). At NTIS, it will be available to the general public, including foreign nations.

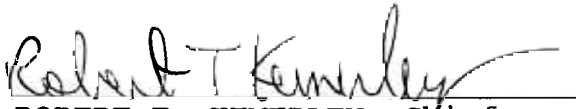
This technical report has been reviewed and is approved for publication.



KEVIN D. LEEDY, Project Engineer  
Aerospace Components Division  
Sensors Directorate



ALAN J. TEWKSBURY, Chief  
Multi-Chip Integration Branch  
Aerospace Components Division



ROBERT T. KEMERLEY, Chief  
Aerospace Components Division  
Sensors Directorate

**IF YOUR ADDRESS HAS CHANGED, IF YOU WISH TO BE REMOVED FROM OUR MAILING LIST, OR IF THE ADDRESSEE IS NO LONGER EMPLOYED BY YOUR ORGANIZATION, PLEASE NOTIFY AFRL/SNDI, WRIGHT-PATTERSON AFB OH 45433-7322 TO HELP MAINTAIN A CURRENT MAILING LIST.**

Copies of this report should not be returned unless return is required by security considerations, contractual obligations, or notice on a specific document.

| <b>REPORT DOCUMENTATION PAGE</b>   |   |   | <i>Form Approved</i><br><i>OMB No. 074-0188</i>  |  |
|--|---|---|--|--|
| Public reporting burden for this collection of information is estimated to average 1 hour per response, including the time for reviewing instructions, searching existing data sources, gathering and maintaining the data needed, and completing and reviewing this collection of information. Send comments regarding this burden estimate or any other aspect of this collection of information, including suggestions for reducing this burden to Washington Headquarters Services, Directorate for Information Operations and Reports, 1215 Jefferson Davis Highway, Suite 1204, Arlington, VA 22202-4302, and to the Office of Management and Budget, Paperwork Reduction Project (0704-0188), Washington, DC 20503  |   |   |  |  |
| <b>1. AGENCY USE ONLY (Leave blank)</b>  | <b>2. REPORT DATE</b><br>September 2001                         | <b>3. REPORT TYPE AND DATES COVERED</b><br>Final, 03/09/1995 – 04/30/2001 |  |  |
| <b>4. TITLE AND SUBTITLE</b><br><br>DEPOSITION AND CHARACTERIZATION OF BARRIER METALS  |   |   | <b>5. FUNDING NUMBERS</b><br>C: In-House<br>PE: 61102F<br>PR: 2300<br>TA: EL<br>WU: 04 |  |
| <b>6. AUTHOR(S)</b><br><br>KEVIN D. LEEDY  |   |   |  |  |
| <b>7. PERFORMING ORGANIZATION NAME(S) AND ADDRESS(ES)</b><br><br>AFRL/SNDI, BUILDING 620<br>2241 AVIONICS CIRCLE, STE. 20<br>WRIGHT-PATTERSON AIR FORCE BASE, OH 45433-7322  |   |   | <b>8. PERFORMING ORGANIZATION REPORT NUMBER</b>  |  |
| <b>9. SPONSORING / MONITORING AGENCY NAME(S) AND ADDRESS(ES)</b><br>SENSORS DIRECTORATE<br>AIR FORCE RESEARCH LABORATORY<br>AIR FORCE MATERIEL COMMAND<br>WRIGHT-PATTERSON AIR FORCE BASE, OH 45433-7318<br>POC: Kevin D. Leedy, AFRL/SNDI, (937) 255-4557 x3490   |   |   | <b>10. SPONSORING / MONITORING AGENCY REPORT NUMBER</b><br><br>AFRL-SN-WP-TR-2001-1107 |  |
| <b>11. SUPPLEMENTARY NOTES</b>   |   |   |  |  |
| <b>12a. DISTRIBUTION / AVAILABILITY STATEMENT</b><br>Approved for public release; distribution unlimited.  |   |   | <b>12b. DISTRIBUTION CODE</b>  |  |
| <b>13. ABSTRACT (Maximum 200 Words)</b><br>Increasing complexity and shrinking sizes of integrated circuits necessitate the development of new materials and processes to meet current system requirements of high performance and reliability in smaller electronic assemblies. In order to achieve the system performance, materials with incompatible physical and electrical properties are often placed into direct contact with one another. Applications such as area array interconnection of Si devices using lead/tin solders, vias in Si integrated circuits and gold contacts to GaAs circuits require the use of barrier metals to physically and chemically separate materials that would otherwise react and form undesirable by-products or significantly decrease the reliability of the electronic system. This effort was initiated in order to advance the understanding of basic mechanisms and influences of processing on the performance of barrier metals. Deposition of the barrier metals was conducted using physical vapor deposition, unique barrier metal alloys that could not be fabricated by thermodynamic equilibrium methods were developed. Characterization of the processing and materials was performed to better understand the essential mechanisms required for high quality barrier metals. |   |   |  |  |
| <b>14. SUBJECT TERMS</b><br>Barrier, physical vapor deposition, thin film  |   |   | <b>15. NUMBER OF PAGES</b><br>38   |  |
|  |   |   | <b>16. PRICE CODE</b>  |  |
| <b>17. SECURITY CLASSIFICATION OF REPORT</b><br>Unclassified   | <b>18. SECURITY CLASSIFICATION OF THIS PAGE</b><br>Unclassified | <b>19. SECURITY CLASSIFICATION OF ABSTRACT</b><br>Unclassified            | <b>20. LIMITATION OF ABSTRACT</b><br>SAR   |  |
| NSN 7540-01-280-5500   |   |   | Standard Form 298 (Rev. 2-89)<br>Prescribed by ANSI Std. Z39-18<br>298-102             |  |

## Table of Contents

|  |    |
|--|----|
| List of Figures .....  | iv |
| List of Tables .....   | vi |
| 1. Summary.....  | 1  |
| 2. Stress, Microstructure And Temperature Stability of Reactive Sputter<br>Deposited Ta(N) Thin Films .....  | 2  |
| 2.1 Abstract .....   | 2  |
| 2.2 Introduction.....  | 2  |
| 2.3 Experiment .....   | 3  |
| 2.4 Results .....  | 4  |
| 2.5 Conclusions .....  | 7  |
| 2.6 References .....   | 7  |
| 3. Stress, Microstructure and Temperature Stability of Reactive Sputter<br>Deposited $WN_x$ Thin Films ..... | 9  |
| 3.1 Abstract .....   | 9  |
| 3.2 Introduction.....  | 9  |
| 3.3 Experiment .....   | 10 |
| 3.4 Results .....  | 10 |
| 3.5 Conclusions .....  | 13 |
| 3.6 References .....   | 14 |
| 4. Organic Solution Deposition of Copper Seed Layers onto Barrier Metals .....                               | 15 |
| 4.1 Abstract .....   | 15 |
| 4.2 Introduction.....  | 15 |
| 4.3 Experiment .....   | 16 |
| 4.4 Results .....  | 17 |
| 4.5 Conclusions .....  | 20 |
| 4.6 References .....   | 20 |
| 5. Properties of Sputtered Bilayer $WN_x/W$ Diffusion Barriers between Si and Cu.....                        | 21 |
| 5.1 Abstract .....   | 21 |
| 5.2 Introduction.....  | 21 |
| 5.3 Experiment .....   | 22 |
| 5.4 Results .....  | 23 |
| 5.5 Conclusions .....  | 26 |
| 5.6 References .....   | 26 |

## List of Figures

| <u>Figure</u>   | <u>Page</u> |
|---|-------------|
| 2.4.1 Nitrogen concentration in Ta(N) films vs. N <sub>2</sub> partial flow rate during deposition.....   | 4           |
| 2.4.2 Resistivity vs. nitrogen concentration in Ta(N) films, as-deposited and after 650°C/5 min. anneal in flowing N <sub>2</sub> .....   | 4           |
| 2.4.3 X-ray diffraction patterns of as-deposited Ta(N) films with various amounts of nitrogen content (at. %) .....   | 5           |
| 2.4.4 X-ray diffraction patterns of Ta(N) films with various amounts of nitrogen content (at. %) after 650°C anneal .....   | 5           |
| 2.4.5 Particle size of Ta(N) films vs. film nitrogen content measured by DF TEM, as-deposited and after 650°C rapid thermal anneal.....   | 6           |
| 2.4.6 Bright field TEM images with inset diffraction patterns of Ta(N) film with 16 at. % nitrogen. As-deposited (L) and after 650°C rapid thermal anneal (R).....                  | 6           |
| 2.4.7 Film stress vs. nitrogen concentration in films, as-deposited and after 650°C anneal.....   | 7           |
| 2.4.8 Stress vs. temperature for Ta(N) films with various nitrogen concentrations .....   | 7           |
| 3.4.1 The W 4p <sub>3/2</sub> and N 1s XPS spectra obtained from the films grown with N <sub>2</sub> partial flows of 0, 8, 16, 30, 40, and 50% .....                               | 11          |
| 3.4.2 The W 4f and 5p <sub>3/2</sub> XPS spectra obtained from the films grown with N <sub>2</sub> partial flows of 0, 8, 16, 30, 40, and 50% .....                                 | 11          |
| 3.4.3 Nitrogen concentrations in WN <sub>x</sub> films as a function of N <sub>2</sub> partial flows during growth.....   | 12          |
| 3.4.4 Bright field TEM images with inset diffraction patterns of WN <sub>x</sub> film with 19 at. % nitrogen. As-deposited (L) and after 650°C rapid thermal anneal (R) ...         | 12          |
| 3.4.5 Particle size of WN <sub>x</sub> films vs. film nitrogen content, as-deposited and after 400 and 650°C rapid thermal anneals .....  | 12          |
| 3.4.6 Film stress vs. nitrogen concentration in 20 nm thick WN <sub>x</sub> films, as-deposited and after 400 and 650°C rapid thermal anneals .....                                 | 13          |
| 3.4.7 Film stress vs. nitrogen concentration in 20 and 200 nm thick WN <sub>x</sub> films, as-deposited and after 650°C furnace anneals .....                                       | 13          |
| 4.4.1 Broadface micrographs of organic solution copper particles on titanium: a) low magnification, b) high magnification. The white or bright areas are the copper particles ..... | 17          |
| 4.4.2 Broadface micrographs of copper films by a) electroless and b) electrolytic plating on top of organic solution copper seeded titanium .....                                   | 18          |
| 4.4.3 Cross sectional micrographs of a) cleaved and b) focus ion beam milled, electrochemically deposited copper on sputter deposited titanium .....                                | 18          |
| 4.4.4 Optical micrographs of patterned titanium/polyimide samples a) as processed and b) after organic solution plus electroless copper deposition.....                             | 19          |

|       |  |    |
|-------|--|----|
| 4.4.5 | Broadface micrographs of sputter deposited TiN after a) copper bearing organic solution processing and b) after subsequent electroless copper deposition.....      | 19 |
| 5.4.1 | Resistivity of $WN_x/W$ and $WN_x/W/Cu$ films, as-deposited and after 650°C anneals .....  | 23 |
| 5.4.2 | X-ray diffraction profiles for selected as-deposited films:<br>a) 20 nm $WN_x/$ 100 nm Cu, b) 10 nm $WN_x/$ 10 nm W/ 100 nm Cu and<br>c) 20 nm W/ 100 nm Cu.....   | 24 |
| 5.4.3 | X-ray diffraction profiles for selected 650°C annealed films:<br>a) 20 nm $WN_x/$ 100 nm Cu, b) 10 nm $WN_x/$ 10 nm W/ 100 nm Cu and<br>c) 20 nm W/ 100 nm Cu..... | 24 |
| 5.4.4 | Cross sectional TEM image of 650°C annealed<br>4 nm $WN_x/$ 16 nm W/ 100 nm Cu.....  | 25 |
| 5.4.5 | (a) SEM image of sputter crater formed in 10 nm $WN_x/$ 10 nm W/ 100 nm Cu structure; (b) AES analysis at points 1-4 marked on SEM.....                            | 25 |
| 5.4.6 | Average stress of $WN_x/W$ and $WN_x/W/Cu$ films, as-deposited and after 650°C anneals .....   | 25 |

## List of Tables

| <b><u>Table</u></b>  | <b><u>Page</u></b> |
|--|--------------------|
| 3.4.1 Crystal structure of $WN_x$ films as-deposited and after 400 and 650°C rapid thermal anneals for 2 min. (a- $WN_x$ , amorphous $WN_x$ )..... | 12                 |
| 5.4.1 Crystal structure of $WN_x/W/Cu$ films as-deposited and after 650°C anneal for 15 min. (a- $WN_x$ , amorphous $WN_x$ ).....                  | 23                 |



## 1. Summary

Increasing complexity and shrinking sizes of integrated circuits necessitate the development of new materials and processes to meet current system requirements of high performance and reliability in smaller electronic assemblies. In order to achieve the system performance, materials with incompatible physical and electrical properties are often placed into direct contact with one another. Applications such as area array interconnection of Si devices using lead/tin solders, vias in Si integrated circuits and gold contacts to GaAs circuits require the use of barrier metals to physically and chemically separate materials that would otherwise react and form undesirable by-products or significantly decrease the reliability of the electronic system. This effort was initiated in order to advance the understanding of basic mechanisms and influences of processing on the performance of barrier metals. Deposition of the barrier metals was conducted using physical vapor deposition (PVD) techniques. Due to the non-equilibrium processing conditions that occur during PVD, unique barrier metal alloys that could not be fabricated by thermodynamic equilibrium methods were developed. Characterization of the processing and materials was performed to better understand the essential mechanisms required for high quality barrier metals.

The accomplishments of this effort are documented in the following papers published in Materials Research Society conference proceedings:

“Stress, Microstructure and Temperature Stability of Reactive Sputter Deposited Ta(N) Thin Films,” Thin Films – Stresses and Mechanical Properties VIII, Vol. 594, Materials Research Society, Pittsburgh, PA (2000).

“Stress, Microstructure and Temperature Stability of Reactive Sputter Deposited  $WN_x$  Thin Films,” Materials, Technology and Reliability for Advanced Interconnects and Low-k Dielectrics, Vol. 612, Materials Research Society, Pittsburgh, PA (2001).

“Organic Solution Deposition of Copper Seed Layers onto Barrier Metals,” Materials, Technology and Reliability for Advanced Interconnects and Low-k Dielectrics, Vol. 612, Materials Research Society, Pittsburgh, PA (2001).

“Properties of Sputtered Bilayer  $WN_x/W$  Diffusion Barriers between Si and Cu,” Materials, Technology and Reliability for Advanced Interconnects and Low-k Dielectrics, Vol. TBD, Materials Research Society, Pittsburgh, PA (in press).

## 2. Stress, Microstructure and Temperature Stability of Reactive Sputter Deposited Ta(N) Thin Films

K. D. Leedy\*, M. J. O'Keefe\*\* and J. T. Grant\*\*\*

\*Air Force Research Laboratory, Sensors Directorate, Wright-Patterson AFB, OH 45433, Kevin.Leedy@wpafb.af.mil

\*\*University of Missouri-Rolla, Dept. of Metallurgical Engineering, Rolla, MO 65409

\*\*\*Research Institute, University of Dayton, Dayton, OH 45469

### 2.1 Abstract

Interest in tantalum nitride thin films for use as diffusion barriers in Cu-based microelectronic interconnects merits the study of tantalum nitride thin film properties as a function of deposition conditions and elevated temperature exposure. In this investigation, the influence of nitrogen content and post deposition annealing on the stress, microstructure and resistivity of Ta(N) films was analyzed. Ta(N) thin films were deposited by reactive dc magnetron sputtering of a Ta target in Ar/N<sub>2</sub> gas mixtures. With an increasing N<sub>2</sub> to Ar flow ratio, the as-deposited crystal structure of the films changed from β-Ta to bcc Ta with N in solid solution to TaN<sub>0.1</sub> to Ta<sub>2</sub>N and finally to TaN. The as-deposited Ta(N) stress, grain size and resistivity of the films were found to be strongly dependent on the phase(s) present. Films with less than 20 at. % nitrogen concentration displayed large compressive stress increases during 650°C anneals in flowing N<sub>2</sub>. Phase transformations to Ta<sub>2</sub>N occurred after 650°C anneals in films with nitrogen concentrations from ~ 15 to 25 at. %. Microstructural characterization using transmission electron microscopy and x-ray diffraction, and chemical analysis by x-ray photoelectron spectroscopy and Auger electron spectroscopy of the Ta(N) films were used to identify the as-deposited and transformed phases.

### 2.2 Introduction

Numerous studies have examined the properties of tantalum and tantalum nitride (Ta(N)) thin films due to their potential application as diffusion barriers between Si and Cu contacts in integrated circuits. An optimal barrier layer should have a dense, amorphous microstructure, a smooth surface morphology, thermal stability with Cu and Si and low film stress [1, 2]. Amorphous thin films are considered more effective diffusion barriers than polycrystalline thin films because of the lack of grain boundaries which function as fast diffusion paths [3]. The thermal stability of Ta(N) films is an important consideration with respect to crystal phase, grain growth, stress and resistivity. Sun [3] investigated the influence of 500 to 800°C vacuum anneals on the structure and composition of Ta(N) films. Stavrev [4] examined the composition and microstructure of TaN films, tetragonal Ta to bcc Ta(N) to fcc TaN. The barrier failure temperature of Ta(N) is not well defined or known. Barrier failure is generally considered to be when Cu has migrated through the barrier to the substrate. Min [5] and Holloway [6] determined that a Ta<sub>2</sub>N diffusion barrier between Si and Cu was stable up to 650°C and 700°C, respectively. Takeyama [7] found a fcc TaN barrier to be stable up to 750°C.

Only limited work has addressed the intrinsic and elevated temperature stress of sputter deposited Ta(N) thin films. Venkatraman [8] showed an as-deposited intrinsic compressive

stress range of 500 to 3000 MPa for reactive sputtered Ta(N) films deposited with 0 to 85 % N<sub>2</sub> in an Ar plasma. Kim [9] measured an as-deposited compressive stress range of 500 to 1200 MPa with 2 to 9 % N<sub>2</sub> in the plasma. Cabral [10] observed the generation of large compressive stresses associated with 400°C anneals on Ta and Ta (2 at. % nitrogen) films and attributed the stress change to oxygen incorporation in the film. Clevenger [11] studied the *in situ* stress and resistance change of Ta thin films as a function of temperature and found a predominant stress relief associated with the transformation of the tetragonal β-Ta phase to the cubic α-Ta phase occurring from 600 to 800°C.

In this paper the microstructure, stress and resistivity of reactive sputtered Ta(N) films in the as-deposited state and after 650°C anneals was studied. The results show that some Ta(N) phases undergo phase transformations at around 550°C while other Ta(N) phases are stable up to 650°C. In addition, annealing induces large compressive stress increases in some Ta(N) films.

### 2.3 Experiment

Tantalum nitride thin films were reactive sputtered from a 99.95% pure Ta target using a Denton Vacuum Discovery 18 dc magnetron sputtering system with a base vacuum of  $1.4 \times 10^{-6}$  Pa. Thermally oxidized (111) silicon wafers of 75 mm diameter and holey carbon support films on 3 mm grids were used as substrate materials during the study. The SiO<sub>2</sub> thickness was 1 μm. A mass flow regulated Ar-N<sub>2</sub> sputtering pressure of ~ 0.53 Pa and 300 W forward power were held constant resulting in a nominal deposition rate of 0.5 nm/s. The N<sub>2</sub> partial flow rate (the ratio of the nitrogen flow rate to the total flow rate of nitrogen and argon) ranged from 0 to 17 %. A water cooled substrate holder was used without external heating for all of the depositions. Films deposited onto the holey carbon grids were 20 nm thick while films deposited onto the Si wafers were 300 to 500 nm thick.

A laser reflectometry Flexus 2900 thin film stress system was used to measure the intrinsic stress of the as-deposited Ta(N) films on the Si substrates and to measure film stress *in situ* during annealing. The nitrogen purged Flexus had a 5°C/min heating rate from 25 to 650°C, a 5 min. hold at 650°C and then a 5°C/min cooling rate to 25°C. Rapid thermal anneals in an AG Associates Heatpulse 210 of films on holey carbon grids were performed at 650°C for 120 sec in flowing Ar-5%H<sub>2</sub> forming gas. X-ray diffraction of 1cm x 1cm samples from the wafers was done using a Rigaku D-MAX III thin film diffractometer with a fixed, low angle (5°) Cu Kα radiation source and a rotating sample holder. Particle sizes were measured using transmission electron microscopy (TEM) of films deposited on holey carbon grids using a Philips CM 200 at 200 kV. Particle sizes were determined by a statistical analysis of grain diameters in bright and dark field broadface images. Film composition was determined with a Physical Electronics model 5700 multiprobe x-ray photoelectron spectroscopy (XPS) system utilizing monochromatic Al Kα radiation. The N 1s photoelectron signal appears as a shoulder on the low binding energy side of the Ta 4p<sub>3/2</sub> signal, and the N 1s signal was retrieved by subtracting the appropriate intensity of the Ta 4p<sub>3/2</sub> signal from a pure Ta film prepared with no nitrogen flow during growth. The Auger electron spectroscopy (AES) measurements were also made using the Physical Electronics model 5700 multiprobe with 10 nA at 5 keV incident electron beam.

## 2.4 Results

### Composition and Resistivity

The film nitrogen concentration measured by AES and XPS versus  $N_2$  partial flow rate during deposition is plotted in Fig. 2.4.1. After an initially high consumption of nitrogen, the films begin to saturate with nitrogen at  $\sim 10\%$   $N_2$  flow rate. Although the general trend in nitrogen content was similar for AES and XPS, the uncertainty in values can be attributed to several items including preferential sputtering, overlap of Ta and N peaks and the application of sensitivity and correction factors. For clarity considerations, only AES values of film nitrogen content are used in subsequent plots.

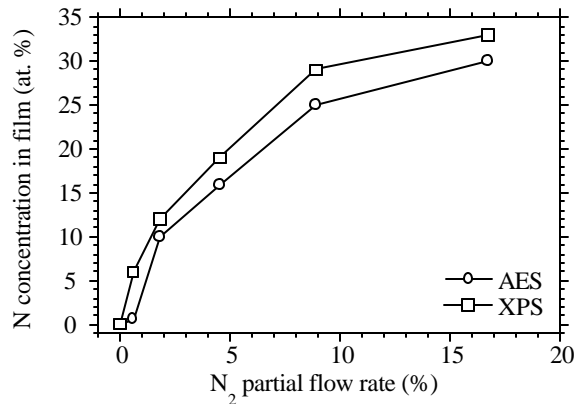


Fig. 2.4.1 Nitrogen concentration in Ta(N) films vs.  $N_2$  partial flow rate during deposition.

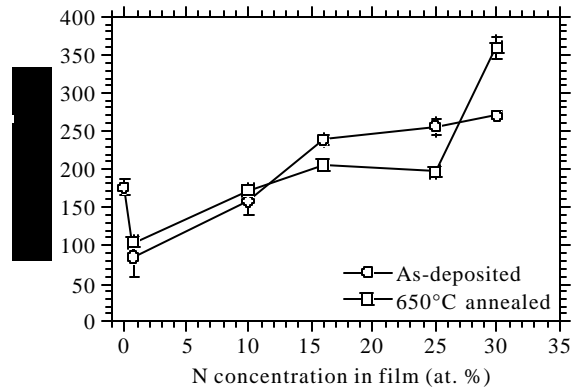


Fig. 2.4.2 Resistivity vs. nitrogen concentration in Ta(N) films, as-deposited and after  $650^\circ\text{C}/5$  min. anneal in flowing  $N_2$ .

The resistivity of tantalum films deposited with no nitrogen flow in the plasma was  $170\ \mu\Omega\text{cm}$ , consistent with the  $\beta$ -Ta phase and confirmed by x-ray diffraction. The  $\beta$ -Ta phase is a metastable tetragonal Ta phase and has been observed in numerous studies [5, 11-14]. As shown in Fig. 2.4.2, as little as 0.7 at. % nitrogen in the film caused a substantial decrease in resistivity to  $70\ \mu\Omega\text{cm}$  and corresponded to a Ta phase change to bcc Ta with likely some nitrogen in solid solution. The difference between  $70\ \mu\Omega\text{cm}$  and the bulk resistivity of Ta of  $13\ \mu\Omega\text{cm}$  is attributed to the fine grain, highly defected thin film structure. With higher nitrogen film concentrations (above 10 at. %), films consisted of tantalum nitride phases with increasing nitrogen contents and correspondingly increased resistivity up to  $250\ \mu\Omega\text{cm}$ . Following  $650^\circ\text{C}$  anneals, films with low nitrogen contents showed slightly increased resistivity while resistivity decreased in intermediate nitrogen content films and started to increase substantially in films with greater than 25 at. % nitrogen. Changes in resistivity are attributed primarily to the differences in resistivity of the transformed crystal structures. Ta and  $\text{Ta}_{0.1}\text{N}$  films exhibited no change in resistivity while  $\text{Ta}_2\text{N}$  film resistivities decreased and TaN film resistivities increased.

### X-ray Diffraction

Figure 2.4.3 shows a sequence of x-ray diffraction patterns from Ta(N) films with a range of nitrogen concentrations. With no nitrogen in the plasma, the film was composed of the metastable  $\beta$ -Ta phase. The addition of 0.7 at. % nitrogen in the film produced a mixture of  $\beta$ -Ta and bcc Ta with nitrogen in solid solution. Film microstructures went from nitrogen-deficient

tantalum nitride phases to nitrogen-rich tantalum nitride phases as film nitrogen content increased. Between 10 and 16 at. % nitrogen film concentrations, films consisted of  $\text{TaN}_{0.1}$  and mixtures of  $\text{TaN}_{0.1}$  and  $\text{Ta}_2\text{N}$ . The  $\text{Ta}_2\text{N}$  and fcc  $\text{TaN}$  phases were present in a 25 at. % nitrogen film. At 30 at. % nitrogen, the only crystalline phase present was  $\text{TaN}$ .

Anneals at  $650^\circ\text{C}$  for 5 min. in the Flexus indicated the phase stability of the various tantalum nitride phases. The nitrogen free  $\beta$ -Ta film crystal structure remained unchanged after  $650^\circ\text{C}$  anneals but transformed completely to bcc Ta after additional annealing at  $775^\circ\text{C}$ , within the same transformation temperature range reported by Clevenger [11]. Figure 2.4.4 shows representative x-ray diffraction patterns of  $650^\circ\text{C}$  annealed  $\text{Ta(N)}$  films. The metastable  $\text{TaN}_{0.1}$  phase persisted nearly completely in a 10 at. % film but decomposed substantially to  $\text{Ta}_2\text{N}$  in a 16 at. % film. A film with nearly the same nitrogen content transformed completely to  $\text{Ta}_2\text{N}$ . The  $\text{TaN}$  crystal structure in the high nitrogen content film (30 at. %) was unaffected by the  $650^\circ\text{C}$  anneal.

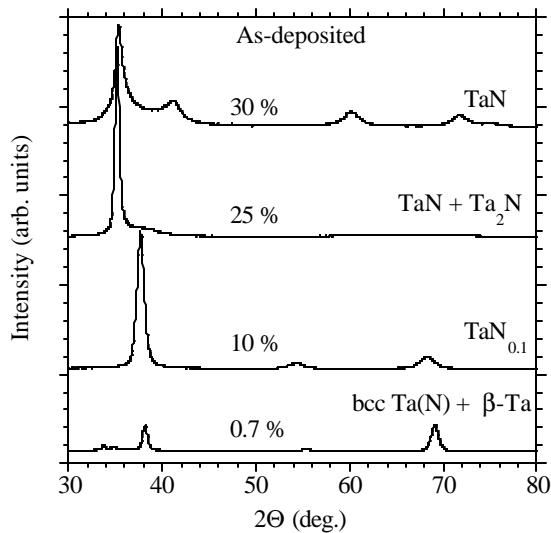


Fig. 2.4.3 X-ray diffraction patterns of as-deposited  $\text{Ta(N)}$  films with various amounts of nitrogen content (at. %).

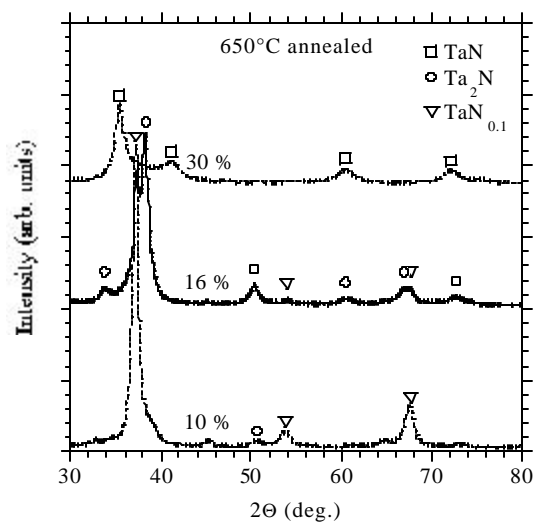


Fig. 2.4.4 X-ray diffraction patterns of  $\text{Ta(N)}$  films with various amounts of nitrogen content (at. %) after  $650^\circ\text{C}$  anneal.

### Particle Size

Particle sizes of  $\text{Ta(N)}$  films were measured by TEM with the results plotted in Fig. 5. The as-deposited film particle sizes decreased from  $\sim 13$  nm to 6 nm with increasing film nitrogen content. Nitrogen is known to decrease grain sizes in physical vapor deposited films. The grain size decrease with increasing film nitrogen content is consistent with a 25 nm to 4 nm reduction observed by Sun [3]. Figures 2.4.5 and 2.4.6 show that anneals at  $650^\circ\text{C}$  caused substantial grain growth in metastable  $\text{Ta(N)}$  films with 10 to 25 at. % nitrogen associated with transformations primarily to  $\text{Ta}_2\text{N}$ . The diffraction patterns on the left and right in Fig. 2.4.6 are of  $\text{TaN}_{0.1}$  and  $\text{Ta}_2\text{N}$ , respectively. The transformed  $\text{Ta}_2\text{N}$  grain sizes were up to 60 nm in diameter in a film with 25 at. % nitrogen. Low and high nitrogen content films showed no measurable grain growth.

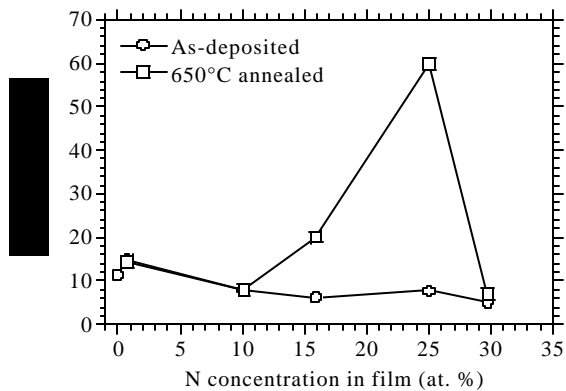


Fig. 2.4.5 Particle size of Ta(N) films vs. film nitrogen content measured by DF TEM, as-deposited and after 650°C rapid thermal anneal.

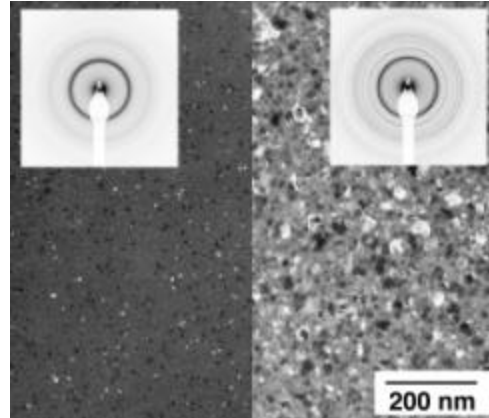


Fig. 2.4.6 Bright field TEM images with inset diffraction patterns of Ta(N) film with 16 at. % nitrogen. As-deposited (L) and after 650°C rapid thermal anneal (R).

### Film Stress

The stress of as-deposited Ta(N) films ranged from approximately 500 MPa tensile to 500 MPa compressive (Fig. 2.4.7). Although the most compressive stresses occurred in films with the highest Ta<sub>2</sub>N phase content, a direct correlation between crystal phase and film stress has not been established.

Following anneals at 650°C, films with low nitrogen concentrations displayed substantial increases in compressive stress. Cabral [10] identified a similar stress change associated with oxygen incorporation in Ta and Ta with 2 at. % nitrogen films during a series of 400°C anneals; AES measurements confirmed the increased oxygen content. In this study surface oxidation manifested as a cloudy haze on films with low nitrogen contents due to oxygen in the Flexus. AES analysis of oxygen concentration in annealed films is ongoing. A film with no nitrogen content delaminated during annealing due to the excessive compressive stress generated (> 3 GPa). However, as film nitrogen content increased, the compressive stress increase became smaller. At approximately 22 at. % nitrogen, the annealed film stress change became tensile and stress in films with higher nitrogen concentrations remained nearly constant at approximately 400 MPa higher than the as-deposited stress. In these films, more tantalum was likely bound in the form of nitride phases so less tantalum was available to getter oxygen.

As shown in Fig. 2.4.8, a slight negative slope in stress vs. temperature plots was observed from 25 to 300°C. Cabral [10] attributed this slope to thermal coefficient of expansion mismatch between the SiO<sub>2</sub> substrate and Ta film at temperatures up to 250°C. More substantial stress changes were observed in films with 15 to 25 at. % nitrogen starting at approximately 450°C: a tensile stress change up to 900 MPa occurred in as little as 8 min. followed by a more gradual compressive stress decrease as the 650°C annealing temperature was approached. The magnitude of this "hump" was most pronounced in films with 25 at. % nitrogen. The stress transition was found to begin at lower temperatures as film nitrogen content increased. We speculate that the "hump" corresponds to the transformation of metastable Ta(N) phases to the Ta<sub>2</sub>N phase based on x-ray diffraction of as-deposited and annealed films. The magnitude of the "hump" parallels the amount of Ta<sub>2</sub>N formed.

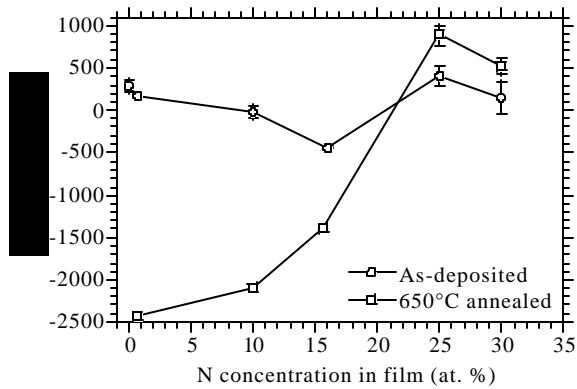


Fig. 2.4.7 Film stress vs. nitrogen concentration in films, as-deposited and after 650°C anneal.

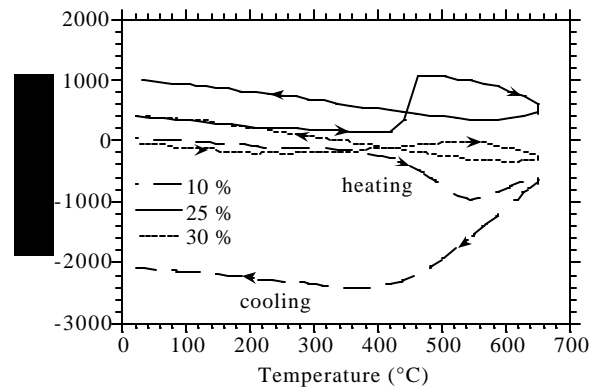


Fig. 2.4.8 Stress vs. temperature for Ta(N) films with various nitrogen concentrations.

## 2.5 Conclusions

Reactive sputtered tantalum nitride thin films displayed a wide range of stable and metastable crystal phases depending on film nitrogen concentration. As-deposited grain sizes were nominally 10 nm for all nitrogen concentrations. Grain growth during 650°C anneals occurred only in films with 15 to 25 at. % nitrogen. The grain size increase to 60 nm was associated with the formation of Ta<sub>2</sub>N. Anneals at 650°C caused substantial compressive stress increases in films with less than 20 at. % nitrogen concentration and modest changes in film resistivity. Further correlation of annealed Ta(N) film oxygen content to compressive stress increases is in progress.

## Acknowledgments

The authors gratefully acknowledge support provided by the Materials and Manufacturing Directorate (J.T.G.) and thank J. Wilson for film depositions.

## 2.6 References

1. S. S. Wong, C. Ryu, H. Lee and K.-W. Kwon in *Advanced Interconnects and Contact Materials and Processes for Future Integrated Circuits*, edited by S. P. Murarka, D. B. Fraser, M. Eizenberg, R. Tung, R. Madar (Mater. Res. Soc. Proc. **514**, Warrendale, PA, 1998) pp. 75-81.
2. B. Chin et al., *Solid State Technol.* **41(7)**, 141 (1998).
3. X. Sun, E. Kolawa, J.-S. Chen, J. S. Reid and M.-A. Nicolet, *Thin Solid Films* **236**, 347 (1993).
4. M. Stavrev, D. Fischer, C. Wenzel, K. Drescher and N. Mattern, *Thin Solid Films* **307**, 79 (1997).
5. K.-H. Min, K.-C. Chun and K.-B. Kim, *J. Vac. Sci. Technol. B* **14(5)**, 3263 (1999).
6. K. Holloway, P. M. Fryer, C. Cabral, J. M. E. Harper, P. J. Bailey and K. H. Kelleher, *J. Appl. Phys.* **71(11)**, 5433 (1992).

7. M. Takeyama, A. Noya, T. Sase and A. Ohta, *J. Vac. Sci. Technol. B* **14(2)**, 674 (1996).
8. R. Venkatraman et al. in *Advanced Interconnects and Contact Materials and Processes for Future Integrated Circuits*, edited by S. P. Murarka, D. B. Fraser, M. Eizenberg, R. Tung, R. Madar (Mater. Res. Soc. Proc. **514**, Warrendale, PA, 1998) pp. 41-52.
9. N. P. Kim, K. L. Coates, G. G. Kunze, C.-P. Chien and M. H. Tanielian, IMAPS Conf, Oct 97, Philadelphia, PA.
10. C. Cabral, L. A. Clevenger and R. G. Schad, *J. Vac. Sci. Technol. B* **12(4)**, 2818 (1994).
11. L. A. Clevenger, A. Mutscheller, J. M. E. Harper, C. Cabral and K. Barmak, *J. Appl. Phys.* **72(10)**, 4918 (1992).
12. K. Radhakrishnan, N. G. Ing and R. Gopalakrishnan, *Mat. Sci. Eng. B* **57**, 224 (1999).
13. R. Saha and J. A. Barnard, *J. Crystal Growth* **174**, 495 (1997).
14. P. Catania, R. A. Roy and J. J. Cuomo, *J. Appl. Phys.* **74(2)**, 1008 (1993).



### 3. Stress, Microstructure and Temperature Stability of Reactive Sputter Deposited $WN_x$ Thin Films

K. D. Leedy, M. J. O'Keefe<sup>1</sup>, J. G. Wilson, R. Osterday<sup>2</sup> and J. T. Grant<sup>3</sup>

Air Force Research Laboratory, Sensors Directorate, Wright-Patterson AFB, OH 45433

<sup>1</sup>University of Missouri-Rolla, Dept. of Metallurgical Engineering, Rolla, MO 65401

<sup>2</sup>Southwestern Ohio Council for Higher Education, Dayton, OH 45420

<sup>3</sup>Research Institute, University of Dayton, Dayton, OH 45469

#### 3.1 Abstract

Tungsten nitride ( $WN_x$ ) thin films can be used as Schottky barriers in high power, high temperature semiconductor devices or as diffusion barriers between Cu, low-k dielectric and silicon because each application requires a thermally stable film. Therefore, it is important to understand the thin film properties of  $WN_x$  as a function of deposition conditions and elevated temperature exposure. In this investigation, the influence of nitrogen content and post deposition annealing on the stress and microstructure of reactive dc magnetron sputter deposited  $WN_x$  films was analyzed. With an increasing  $N_2$  to Ar flow ratio, the as-deposited crystal structure of the films changed from  $\alpha$ -W to  $\beta$ -W to amorphous  $WN_x$  and finally to  $W_2N$ . Rapid thermal anneals up to 650°C resulted in large tensile stress increases and phase transformations to  $W_2N$  in the nitrogen-containing films. Grain growth during annealing decreased as the concentration of nitrogen in the film increased. The nitrogen content in the films was determined using x-ray photoelectron spectroscopy (XPS).

#### 3.2 Introduction

Tungsten nitride thin films have been studied extensively for use as thermally stable Schottky contacts to GaAs [1-4]. Another potential application of  $WN_x$  is as a barrier to Cu diffusion in Si-based integrated circuits. An optimal barrier layer should have a dense, amorphous microstructure, a smooth surface morphology, thermal stability with Cu and Si, low film stress and minimal thickness (10 to 20 nm) [5, 6]. Amorphous thin films are considered more effective diffusion barriers than polycrystalline thin films because of the lack of grain boundaries which function as fast diffusion paths [7]. Several transition metals and their nitrides are good candidate materials, including tungsten nitride [8]. Because of high temperature anneals used in the fabrication of semiconductor devices, the thermal stability of  $WN_x$  films is an important consideration with respect to crystallinity, grain growth and stress.

Fabrication methods for  $WN_x$  films include metal-organic chemical vapor deposition [9], plasma enhanced chemical vapor deposition (PECVD) [10, 11] and reactive sputtering [12-14]. Lee [15] investigated PECVD  $WN_x$  as a diffusion barrier between Al and Si while So [13] studied reactive sputtered  $WN_x$ . The Cu barrier performance of reactive sputtered  $WN_x$  was examined by Uekubo [14] with 25 nm thick  $WN_x$  films and Suh [12] with 5 to 100 nm  $WN_x$  thick films. Alternatively, a large grained reactive sputtered  $WN_x$  film fabricated by Yongjun [16] exhibited low stress, high surface smoothness and high thermal stability. It was found that a low nitrogen concentration in a W seed layer followed by a rapid thermal anneal in  $N_2$  formed a large grained  $WN_x$  barrier.

The intrinsic stress of  $WN_x$  thin films has been addressed in only limited studies. Yu [1] measured a compressive stress range of  $\sim 3$  to 1.75 GPa in 300 nm thick  $WN_x$  films deposited at 5 mTorr with  $N_2$  partial flows from 0 to 40 %. Lee [10] studied the influence of PECVD  $W/WN_x$  bilayers on the intrinsic film stress.

In this paper the influence of film thickness and nitrogen content on the microstructure and stress of reactive sputtered  $WN_x$  films in the as-deposited state and after 400 and 650°C anneals was studied.

### 3.3 Experiment

Tungsten nitride thin films were deposited from a 99.95% pure W target using a Denton Vacuum Discovery 18 dc magnetron sputtering system with a base vacuum of  $1.4 \times 10^{-6}$  Pa. A mass flow regulated Ar- $N_2$  sputtering pressure of  $\sim 0.53$  Pa and 250 W forward power were held constant resulting in a nominal deposition rate of 0.3 nm/s. The  $N_2$  partial flow rate (the ratio of the nitrogen flow rate to the total flow rate of nitrogen and argon) ranged from 0 to 50 %. Thermally oxidized (100) silicon wafers of 75 mm diameter and holey carbon support films on 3 mm grids were used as substrate materials during the study. Films deposited onto the holey carbon grids were 20 nm thick while films deposited onto the Si wafers were either 20 or 200 nm thick. A water-cooled substrate holder was used without external heating for all of the depositions.

The intrinsic stress of the  $WN_x$  films was calculated using the wafer curvature technique and Stoney's equation. A laser reflectometry Flexus 2900 thin film stress system was used to measure the intrinsic stress of the as-deposited  $WN_x$  films on the Si substrates and to measure film stress *in-situ* during annealing. The nitrogen purged Flexus had a 5°C/min heating rate from 25 to 650°C, a 5 min. hold at 650°C and then a 5°C/min cooling rate to 25°C. Rapid thermal anneals of films on holey carbon grids were performed in an AG Associates Heatpulse 210 at 400 and 650°C for 120 sec in flowing Ar-5% $H_2$  forming gas. X-ray diffraction (XRD) of 200 nm thick samples was done using a Rigaku D-MAX III thin film diffractometer with a fixed, low angle (5°) Cu  $K\alpha$  radiation source and a rotating sample holder. Particle size and crystal structure of 20 nm thick films were measured by transmission electron microscopy (TEM) using a Philips CM 200 at 200 keV. Particle sizes were determined by a statistical analysis of grain diameters in bright and dark field broadface images. Film composition was determined with a Physical Electronics model 5700 x-ray photoelectron spectroscopy (XPS) system utilizing monochromatic Al  $K\alpha$  radiation.

### 3.4 Results

#### Composition

The atomic concentration of nitrogen in the films was determined from XPS measurements. These measurements were made several weeks after the films had been grown, so the surfaces were affected by the atmospheric environment in which they had been stored. XPS analysis showed that the surfaces were oxidized and contaminated with carbon. The W  $4p_{3/2}$  and N 1s photoelectron signals obtained from these surfaces are shown in Fig. 3.4.1, and were used for the quantitative analysis. (Note that the spectra have been offset for clarity). Since the W  $4p_{3/2}$  and N 1s photoelectrons have similar kinetic energies, about 1060 and 1090 eV

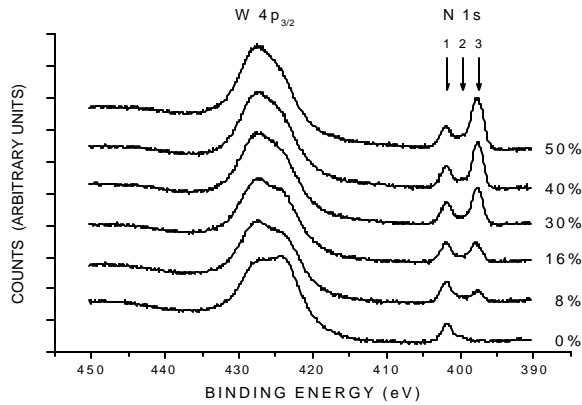


**Figure 3.4.1** The W 4p<sub>3/2</sub> and N 1s XPS spectra obtained from the films grown with N<sub>2</sub> partial flows of 0, 8, 16, 30, 40, and 50%.

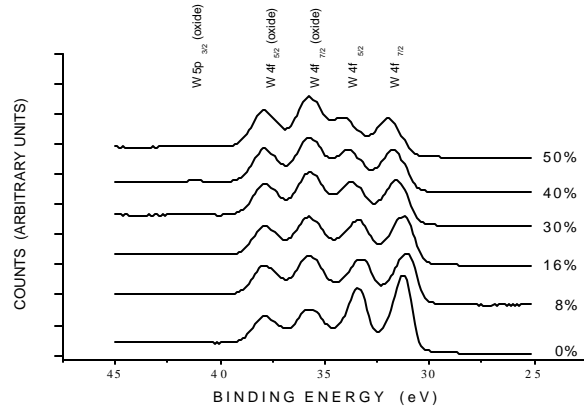


**Figure 3.4.2** The W 4f and 5p<sub>3/2</sub> XPS spectra obtained from the films grown with N<sub>2</sub> partial flows of 0, 8, 16, 30, 40, and 50%.

respectively, their intensities will be similarly attenuated by surface contamination. The N 1s signals are comprised of three peaks (1, 2, and 3). The intensities of peaks 1 and 2 from each sample are fairly constant, whereas the intensities of peak 3 increase with N<sub>2</sub> flow rate. Peak 3 corresponds to nitrogen in the film, whereas peaks 1 and 2 are due to surface reactions where the nitrogen is in a higher oxidation state. (Carbon and the nitrogen peaks 1 and 2 all decreased very rapidly with inert gas sputtering of the surface). The W 4p<sub>3/2</sub> lineshape also varies between samples and is due to different degrees of surface oxidation of the films. The degree of surface oxidation was determined from the W 4f and 5p<sub>3/2</sub> photoelectron spectra, as these peaks are relatively sharp and shifted to higher binding energy due to surface oxidation. These W spectra are shown in Fig. 3.4.2. The fractions of the total non-oxide tungsten signals obtained from the W 4f and 5p<sub>3/2</sub> (barely visible in the figure) spectra were then applied to the total W 4p<sub>3/2</sub> intensity to remove the amount due to surface oxidation. The nitrogen concentrations in the films were then obtained by calculation using Scofield cross-sections, and asymmetry parameter, analyzer transmission and atom size corrections [17], and are plotted in Fig. 3.4.3. The increase in film nitrogen content is also reflected by an increase in resistivity from 16 to 244 μΩ·cm for 0 and 43 at. % nitrogen films, respectively.

### Microstructure

The crystal structure of as-deposited WN<sub>x</sub> films with no nitrogen was bcc α-W and remained α-W after rapid thermal anneals of 400 and 650°C. Films with 12 at. % nitrogen were β-W (A-15) and transformed completely to W<sub>2</sub>N after 650°C anneals. Films with 29 and 35 at. % nitrogen had a predominantly amorphous structure in the as-deposited condition and after 400°C anneals. The W<sub>2</sub>N phase existed in the as-deposited and annealed 43 at. % nitrogen films. All films with nitrogen contained W<sub>2</sub>N after 650°C anneals and films with > 29 at. % nitrogen exhibited some conversion of W<sub>2</sub>N to α-W after 650°C anneals. The conversion of WN<sub>x</sub> to α-W due to annealing was studied extensively by Lin [11, 18]. A phase map by Suh [12] shows the same general trend in WN<sub>x</sub> microstructure evolution with temperature using 450 to 850°C furnace anneals for 1 hr. As-deposited and furnace annealed WN<sub>x</sub> data from Yu [1] at 700°C/30 min. also exhibited the same type of crystal structure development. Table 3.4.1 shows the WN<sub>x</sub>

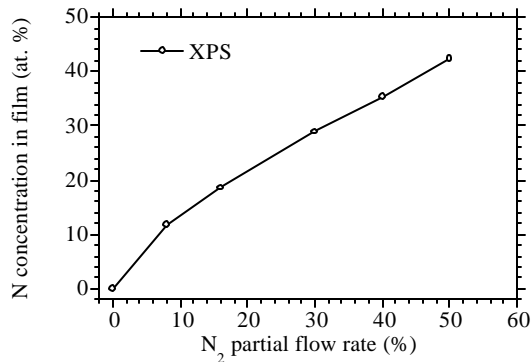


**Figure 3.4.3** Nitrogen concentrations in  $WN_x$  films as a function of  $N_2$  partial flows during growth.

| Nitrogen Content (at. %) | As-deposited            | 400°C                    | 650°C                |
|--------------------------|-------------------------|--------------------------|----------------------|
| 0                        | $\alpha$ -W             | $\alpha$ -W              | $\alpha$ -W          |
| 12                       | $\beta$ -W              | $\beta$ -W + $\alpha$ -W | $W_2N$               |
| 19                       | a- $WN_x$ + $\alpha$ -W | $\beta$ -W + $\alpha$ -W | $W_2N$               |
| 29                       | a- $WN_x$               | a- $WN_x$                | $\alpha$ -W + $W_2N$ |
| 35                       | a- $WN_x$ + $W_2N$      | a- $WN_x$ + $W_2N$       | $W_2N$ + $\alpha$ -W |
| 43                       | $W_2N$                  | $W_2N$                   | $W_2N$ + $\alpha$ -W |

**Table 3.4.1** Crystal structure of  $WN_x$  films as-deposited and after 400 and 650°C rapid thermal anneals for 2 min. (a- $WN_x$ , amorphous  $WN_x$ ).

crystal phases of the 20 nm thick as-deposited and rapid thermal annealed films. For films with multiple phases present, the first species listed was most prevalent. XRD of 200 nm thick  $WN_x$  films showed the same structures.

$WN_x$  particles were 5 to 10 nm in diameter in the as-deposited state. Figures 3.4.4 and 3.4.5 show that rapid thermal anneals caused grain growth in films with lower nitrogen contents, associated primarily with transformations to  $W_2N$ . The diffraction patterns on the left and right in Fig. 3.4.4 are of amorphous  $WN_x$  and  $W_2N$ , respectively. The highest nitrogen content films showed no measurable grain growth after anneals, attributed to the stability of  $W_2N$ . Accurate grain size measurements in films with no nitrogen were complicated by a nonuniform morphology. Although some of the  $WN_x$  films are listed as amorphous, ~ 10 nm diameter particles were observed and measured.

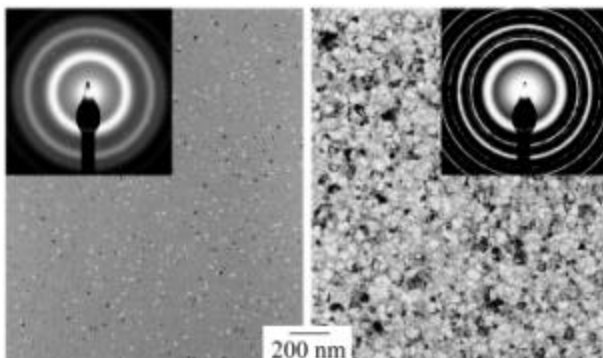


**Figure 3.4.4** Bright field TEM images with inset diffraction patterns of  $WN_x$  film with 19 at. % nitrogen. As-deposited (L) and after 650°C rapid thermal anneal (R).

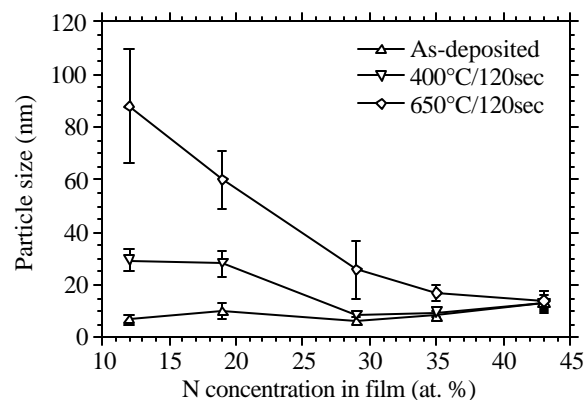


**Figure 3.4.5** Particle size of  $WN_x$  films vs. film nitrogen content, as-deposited and after 400 and 650°C rapid thermal anneals.

## Film Stress

As-deposited 20 nm thick  $WN_x$  films exhibited compressive intrinsic stresses that became more compressive with increasing film nitrogen content. Figure 3.4.6 shows stress as a function of nitrogen content for as-deposited films and films subjected to rapid thermal anneals at 400 and 650°C. The rapid thermal anneals resulted in tensile stress increases in all films with a maximum increase of > 2000 MPa compared to the as-deposited films. Factors contributing to the generation of tensile stress include grain growth [19] and differential thermal expansion between the film and substrate.

The difference in intrinsic stress between 20 and 200 nm thick  $WN_x$  films is shown in Fig. 3.4.7. As-deposited stresses of both thickness films were similar except in lower nitrogen content films where 200 nm films exhibited more tensile stresses. Furnace anneals at 650°C resulted in large tensile stress increases in 200 nm thick  $WN_x$  films while the only significant stress change in 20 nm thick  $WN_x$  was a tensile increase in 43 at. % nitrogen films. Furnace anneals were performed in flowing  $N_2$ , so the propensity for film oxidation is higher than in the forming gas used in rapid thermal anneals.

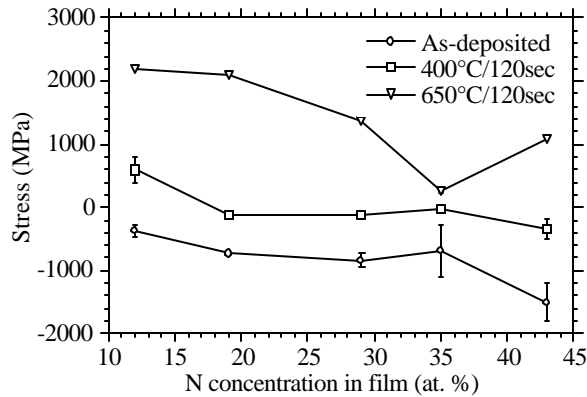


**Figure 3.4.6** Film stress vs. nitrogen concentration in 20 nm thick  $WN_x$  films, as-deposited and after 400 and 650°C rapid thermal anneals.

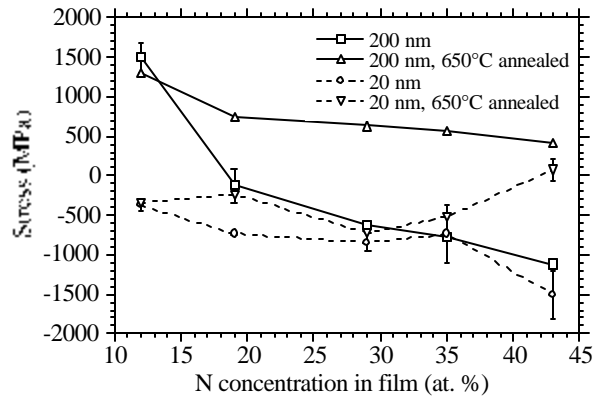


**Figure 3.4.7** Film stress vs. nitrogen concentration in 20 and 200 nm thick  $WN_x$  films, as-deposited and after 650°C furnace anneals.

## 3.5 Conclusions

Reactive sputter deposited tungsten nitride thin films displayed a range of stable and metastable crystal phases depending on film nitrogen concentration, from  $\alpha$ -W with no nitrogen concentration to  $W_2N$  at high nitrogen concentrations. XPS was used to calculate the film nitrogen contents. As-deposited particle sizes were nominally 10 nm for all nitrogen concentrations. Maximum grain growth up to 90 nm after 400 and 650°C rapid thermal anneals occurred in films with the lowest nitrogen contents. Rapid thermal anneals and furnace anneals at 650°C caused substantial tensile stress increases in most films, decreasing grain growth with increasing nitrogen concentration, and a predominantly  $W_2N$  crystal structure.

## Acknowledgments

The authors gratefully acknowledge support provided by the Materials and Manufacturing Directorate (J.T.G.).

## 3.6 References

1. K. M. Yu, J. M. Jaklevic, E. E. Haller, S. K. Cheung and S. P. Kwok, *J. Appl. Phys.* **64(3)**, 1284 (1988).
2. Y. T. Kim and C. W. Lee, *J. Appl. Phys.* **76(1)**, 542 (1994).
3. A. E. Geissberger, R. A. Sadler, F. A. Leyenaar and M. L. Balzan, *J. Vac. Sci. Technol. A* **4(6)**, 3091 (1986).
4. J. S. Lee, C. S. Park, J. W. Yang, J. Y. Kang and D. S. Ma, *J. Appl. Phys.* **67(2)**, 1134 (1990).
5. S. S. Wong, C. Ryu, H. Lee and K.-W. Kwon in *Advanced Interconnects and Contact Materials and Processes for Future Integrated Circuits*, edited by S. P. Murarka, D. B. Fraser, M. Eizenberg, R. Tung, R. Madar (Mater. Res. Soc. Proc. **514**, Warrendale, PA, 1998) pp. 75-81.
6. B. Chin et al., *Solid State Technol.* **41(7)**, 141 (1998).
7. X. Sun, E. Kolawa, J.-S. Chen, J. S. Reid and M.-A. Nicolet, *Thin Solid Films* **236**, 347 (1993).
8. C. Galewski and T. Seidel, *European Semiconductor Design Production Assembly* **21(1)**, 31 (1999).
9. J. E. Kelsey, C. Goldberg, G. Nuesca, G. Peterson and A. E. Kaloyeros, *J. Vac. Sci. Technol. B* **17(3)**, 1101 (1999).
10. C. W. Lee and Y. T. Kim, *Appl. Phys. Lett.* **65(8)**, 965 (1994).
11. J. Lin, A. Tsukune, T. Suzuki and M. Yamada, *J. Vac. Sci. Technol. A* **17(3)**, 936 (1999).
12. B.-S. Suh, Y.-J. Lee, J.-S. Hwang and C.-O. Park, *Thin Solid Films* **348**, 299 (1999).
13. F. C. T. So, E. Kolawa, X.-A. Zhao, E. T.-S. Pan and M.-A. Nicolet, *J. Appl. Phys.* **64(5)**, 2787 (1988).
14. M. Uekubo, T. Oku, K. Nii, M. Murakami, K. Takahiro, S. Yamaguchi, T. Nakano and T. Ohta, *Thin Solid Films* **286**, 170 (1996).
15. C. W. Lee, Y. T. Kim, C. Lee, J. Y. Lee, S.-K. Min and Y. W. Park, *J. Vac. Sci. Technol. B* **12(1)**, 69 (1994).
16. H. Yongjun, U. S. Patent No. 5633200, 1997.
17. M.P. Seah in *Practical Surface Analysis, 2<sup>nd</sup> Ed., Vol.1, Auger and X-ray Photoelectron Spectroscopy*, ed. by D. Briggs and M.P. Seah, (John Wiley, Chichester, 1990), Chapter 5.
18. J. Lin, A. Tsukune, T. Suzuki and M. Yamada, *J. Vac. Sci. Technol. A* **16(2)**, 611 (1998).
19. F. Spaepen, *Acta Mater.* **48**, 31 (2000).

## 4. Organic Solution Deposition of Copper Seed Layers onto Barrier Metals

H. Gu, R. Fang, T. J. O'Keefe, M. J. O'Keefe, W.-S. Shih<sup>1</sup>, J. A. M. Snook<sup>1</sup>, K. D. Leedy<sup>2</sup> and R. Cortez<sup>2</sup>

University of Missouri-Rolla, Dept. of Metallurgical Engineering and Materials Research Center, Rolla, MO 65409, U.S.A.

<sup>1</sup>Brewer Science, Inc., Rolla, MO 65401, U.S.A.

<sup>2</sup>Air Force Research Laboratory, Sensors Directorate, Wright-Patterson AFB, OH 45433, U.S.A

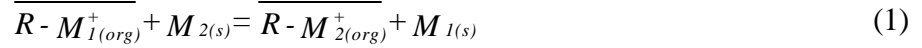
### 4.1 Abstract

Spontaneous deposition of copper seed layers from metal bearing organic based solutions onto sputter deposited titanium, titanium nitride, and tantalum diffusion barrier thin films has been demonstrated. Based on electrochemically driven cementation exchange reactions, the process was used to produce adherent, selectively deposited copper metal particulate films on blanket and patterned barrier metal thin films on silicon substrates. The organic solution deposited copper films were capable of acting as seed layers for subsequent electrolytic and electroless copper deposition processes using standard plating baths. Electroless and electrolytic copper films from 0.1 $\mu\text{m}$  to 1.0 $\mu\text{m}$  thick were produced on a variety of samples on which the organic solution copper acted as the initial catalytic seed layer. The feasibility of using organic solution deposited palladium as a seed layer followed by electroless copper deposition has also been demonstrated. In addition, experiments conducted on patterned barrier metal samples with exposed areas of dielectric such as polyimide indicated that no organic solution copper or palladium deposition occurred on the insulating materials.

### 4.2 Introduction

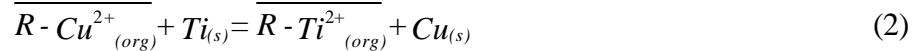
The incorporation of low-k dielectrics and copper interconnects in the fabrication of high speed silicon integrated circuits (ICs) requires significant changes to the current method of using blanket deposition and etch back processes. While physical vapor deposition (PVD) techniques, such as sputtering, appear to be viable for the formation of thin barrier layers between the low-k dielectric and copper interconnect, technical and economic benefits of using chemical vapor deposition (CVD) [1], electrolytic plating [2], and electroless plating [3] processes for build up of the copper interconnects make these approaches attractive alternatives. Electrochemical deposition of copper is relatively inexpensive compared to vapor deposition methods but suffers from the fact that the barrier layers, typically titanium or tantalum based metals or metal nitrides, are difficult to electrochemically activate and plate with adherent copper. In fact, in the primary electrolytic copper metals industry, titanium is employed as a re-usable cathode material because the copper is easily removed from the titanium surface after plating. Therefore, it is necessary to deposit adherent, thin seed layers of copper onto the barrier layer prior to deposition of thicker copper films by electrochemical methods. Although PVD and CVD copper seed layers can be used to fabricate electroplated copper interconnects, an electrochemical process for depositing copper seed layers and interconnects has many benefits, including lower cost of ownership, simplified processing parameters, and the ability to scale with increasing wafer size [4].

Traditional electrochemical deposition of metal films and coatings utilizes aqueous electrolytes. A novel process for depositing metals from organic solutions based on cementation exchange reactions has been demonstrated for a number of metal/metal ion systems, including Au on Zn and Pb on Fe [5,6]. Most of the previous work on electrochemical deposition of metals from organic solutions has focused on copper deposition onto sputtered aluminum thin films [7]. In general, the cementation exchange reaction is based on the dissolution of a less noble metal substrate material ( $M_2$ ) into the organic solution ( $R-M_{x(org)}$ ) while simultaneously depositing more noble metal atoms ( $M_1$ ) onto the surface of the substrate [5]:



An inherent characteristic of the process is high selectivity of the depositing atoms as the cementation exchange reaction occurs only at the surface of electrochemically active, less noble cathodic sites and not on insulating or dielectric materials. In contrast, standard palladium activation from aqueous stannous chloride/palladium solutions that catalyze electroless copper deposition can be used on both conducting (metal) and non-conducting (polymer) surfaces since it is not selective to the underlying substrate material.

In this study, we report for the first time the use of organic solution deposition of copper onto barrier metals such as Ti, TiN and Ta, for example



in which adherent Cu seed layers are deposited onto sputter deposited barrier metal films. To demonstrate the feasibility of the seed layers with subsequent electrochemical copper deposition, standard electroless and electrolytic copper plating solutions were used to build up 0.1 $\mu$ m to 1.0 $\mu$ m thick copper layers on the barrier films after deposition of the catalytic seed layers.

### 4.3 Experiment

Deposition of Ti, TiN and Ta barrier films onto Si or SiO<sub>2</sub> wafer substrates was done using a Denton Vacuum Discovery 18 dc magnetron sputtering system with a base vacuum of 1.4 x 10<sup>-6</sup> Pa. The pressure in the chamber was held constant at ~0.53 Pa during deposition and the forward power was fixed at 300W. Titanium and tantalum films were deposited using argon gas while the TiN was reactively deposited using an Ar/N<sub>2</sub> mixture. A water cooled substrate holder was used without external heating for all of the depositions. Film thickness was varied from 50nm to 1000nm. Patterning of 100nm Ti films was accomplished by contact lithography. Polyimide dielectric which was spin coated, exposed and cured over the patterned Ti lines and bond pads was left on the substrates during subsequent electrochemical plating operations.

Copper seed layer deposition onto the barrier metal films was done for less than one minute using organic solutions in which the copper ion concentration was < 1 g/L. Subsequent electroless copper deposition was accomplished using a formaldehyde based aqueous formulation of 10-15 g/L copper sulfate (CuSO<sub>4</sub>-5H<sub>2</sub>O), 40 g/L Na<sub>2</sub>EDTA (ethylenediamine tetra-acetate), 10-15 g/L formaldehyde, 12 g/L NaOH to pH of 12.5, 65°C bath temperature for 10 minutes. A copper plating bath consisting of 180 g/L copper sulfate (CuSO<sub>4</sub>-5H<sub>2</sub>O), 65 g/L H<sub>2</sub>SO<sub>4</sub>, 60 parts per million chloride, and brightener and leveler additives at 35°C was used to deposit electrolytic films at a current density of 25 mA/cm<sup>2</sup> for 5 minutes.



Analysis of the deposited films was done using two different scanning electron microscopes. A Hitachi S4700 field emission microscope and a FEI Dual Beam 620 focused ion beam (FIB) microscope were used to image and conduct chemical analysis of broadface and cross-sectional samples after deposition.

#### 4.4 Results

Attempts to directly deposit copper onto the different barrier metals using only the electroless and electrolytic copper plating baths were unsuccessful. In all cases, either no copper plated on the surface or the copper film that did plate on the surface was not adherent. This result was expected since Ti and Ta surfaces are normally not receptive to deposition of adherent copper films by electrochemical plating operations without special surface preparation. Results from organic solution treated barrier metal films will be presented by the type of barrier film.

##### Ti Films

In this study preliminary investigations on organic solution deposited copper onto barrier films has focused on sputter deposited titanium. Although not normally used as a barrier film, Ti is often used as an adhesion and/or protection layer for metallic films such as aluminum and TiN. For the purposes of this study, it served the role of a reproducible, model surface for conducting organic solution deposition experiments.

Depicted in Fig. 4.4.1a and 4.4.1b are broadface scanning electron microscope (SEM) micrographs of organic solution deposited copper particles on the surface of a 1000nm thick Ti film. The light or white particles in Fig. 4.4.1 are the deposited copper. As can be seen in Fig. 4.4.1a, the distribution of sub-micrometer size copper particles on the surface of the Ti is fairly uniform. Fig. 4.4.1b is a higher magnification of the same sample in which the largest copper particle is approximately 400nm in diameter with a typical copper particle size of <100nm. Adherence tape testing of the seed layers after organic solution deposition indicated that the copper particles could not be removed from the titanium. Chemical characterization of the large particles by energy dispersive x-ray analysis indicated only a copper signal.

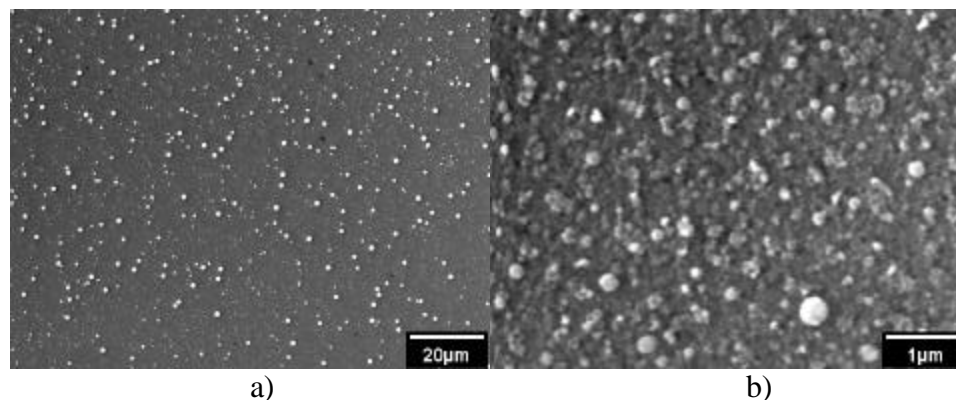


**Figure 4.4.1.** Broadface micrographs of organic solution copper particles on titanium: a) low magnification, b) high magnification. The white or bright areas are the copper particles.

After deposition of the copper seed layers from organic solutions, the Ti barrier film samples were subjected to electroless and electrolytic plating. Depicted in Fig. 4.4.2a is a broadface SEM micrograph after organic seed layer and electroless copper deposition while Fig. 4.4.2b is after organic seed layer and electrolytic copper plating. Both organic solution seed layer/aqueous electrochemical copper samples passed qualitative adherence testing of the samples using standard scotch tape.

As presented in equation (2), an inherent part of the process is dissolution of the barrier film into the organic solution. Lack of uniformity or preferential attack of the barrier film is undesirable from a reliability standpoint. Figs. 4.4.3a and 4.4.3b are cross-sectional micrographs from a 1000nm thick Ti film sample after a three step copper deposition process: first, organic copper seed layer, then electroless copper deposition, and finally electrolytic copper deposition. Fig. 4.4.3a is the sample after cleaving the wafer while Fig. 4.4.3b is a similar sample that was ion milled in the FIB microscope. Both figures demonstrate that a continuous, void free copper film was electrochemically deposited on the sputter deposited Ti film. Examination of similar samples prepared on 100nm thick Ti films gave the same results in that adherent, void free copper was deposited on the barrier film without appreciable or non-uniform removal of the Ti layer.

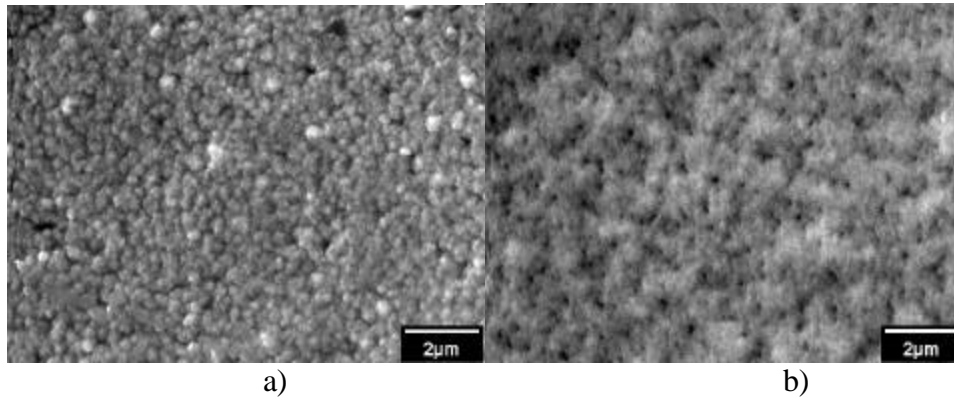


**Figure 4.4.2.** Broadface micrographs of copper films by a) electroless and b) electrolytic plating on top of organic solution copper seeded titanium.

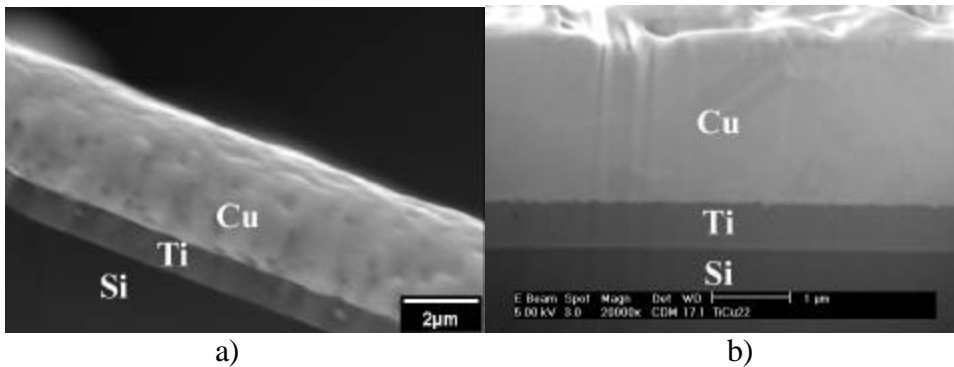


**Figure 4.4.3.** Cross sectional micrographs of a) cleaved and b) focus ion beam milled, electrochemically deposited copper on sputter deposited titanium.

The previous Ti barrier film results were on unpatterned wafers. As mentioned in the introduction, the process is inherently area selective in that deposition should only occur on electrochemically active, less noble metal surfaces. Patterned Ti films on Si/SiO<sub>2</sub> wafers with polyimide as the dielectric were subjected to a copper bearing organic solution and then an electroless copper plating bath. Shown in Fig. 4.4.4a is a section of the wafer before exposure to the electrochemical deposition solutions while Fig. 4.4.4b is the same area of the wafer after copper deposition. Although difficult to show without a color micrograph, copper was deposited on top of all of the exposed Ti in Fig. 4.4.4b. No copper was deposited on the polyimide. Similar experiments that used dielectrics such as Si<sub>3</sub>N<sub>4</sub> and benzocyclobutene (BCB) had comparable results: copper deposited only on the exposed metal and not on the dielectric.

Preliminary results using Pd loaded organic solutions, in place of the copper loaded organic solutions, have paralleled the copper seed layer experiments on titanium. After organic Pd seed layer processing the Ti surface could be selectively plated with electroless copper.

### TiN Films

Attempts to produce copper seed layers on the surface of 50nm to 100nm thick TiN layers have been dependent on the structure, phase and nitrogen content of the TiN. Adjustments to the chemical composition of the organic solution have been required in order to use Cu or Pd to activate the TiN surface for subsequent electroless or electrolytic copper plating. Preliminary analysis of the surface of the TiN after organic solution copper deposition indicates the surface is devoid of any distinguishing features showing copper nuclei (Fig. 4.4.5a) but that after electroless copper deposition the film surface appears similar to the Ti samples (Fig. 4.4.5b). The electroless copper is essentially void free and adherent to the underlying substrate.

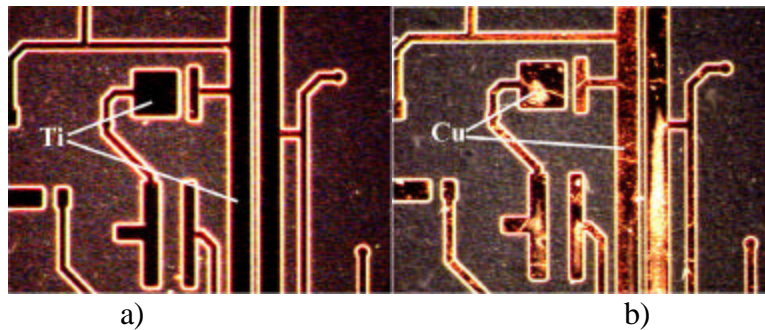


**Figure 4.4.4.** Optical micrographs of patterned titanium/polyimide samples a) as processed and b) after organic solution plus electroless copper deposition.

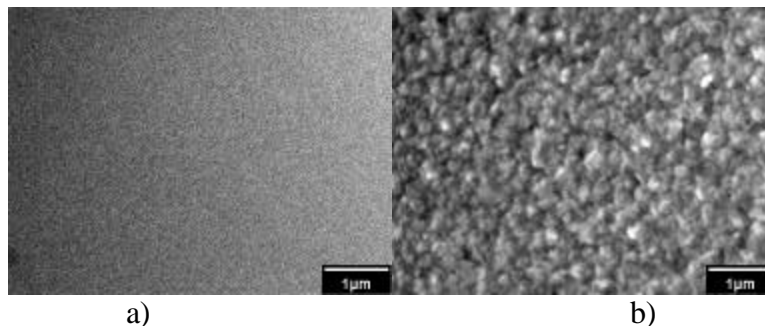


**Figure 4.4.5.** Broadface micrographs of sputter deposited TiN after a) copper bearing organic solution processing and b) after subsequent electroless copper deposition.

## Ta Films

Work has only recently been started using metal bearing organic solutions to deposit seed layers on Ta and Ta(N) barrier films. Initial screening tests indicate that the process is feasible but the passivity of the tantalum films is much more tenacious than titanium films, requiring a more aggressive media to remove the surface oxide layer. However, non-uniform seed layers have been deposited and subsequently plated with electroless copper in localized areas. Studies to improve deposition uniformity and adherence have been initiated.

## 4.5 Conclusions

A spontaneous, electrochemically driven process for activating the surface of Ti, TiN and Ta barrier films for subsequent electroless and electrolytic copper plating processes has been demonstrated. Organic based solutions with dissolved copper were used to activate and catalyze the surface of the barrier metals which resulted in adherent copper seed layers compatible for use with standard electroless and electrolytic plating baths. Void free copper films with a final thickness of up to 1  $\mu\text{m}$  were deposited onto the barrier films. Selective area deposition of organic solution and then electroless copper onto the exposed surface of patterned titanium/polyimide samples indicated that deposition occurred only on the metal and not the dielectric. Preliminary results using palladium loaded organic solutions indicated the feasibility of using alternative metal systems to activate the surface of barrier metals for subsequent electroless copper deposition.

## Acknowledgments

This work was funded by the Small Business Innovation Research (SBIR) program through the Sensors Directorate of the Air Force Research Laboratory, contract # F33615-97-C-1074.

## 4.6 References

1. C. Ryu, K.-W. Kwon, A. L. S. Loke, H. Lee, T. Nogami, V. M. Dubin, R. A. Kavari, G. W. Way, and S. S. Wong, *IEEE Transactions on Electron Devices* **46**(6), 1113 (1999).
2. R. D. Mikkola, Q.-T. Jiang, and B. Carpenter, *Plating & Surface Finishing*, March, 81 (2000).
3. V. Dubin and S.-D. Yosi, *J. Electrochem. Soc.* **44**(3), 898 (1997).
4. T. J. O'Keefe, M. Stroder, M. J. O'Keefe in *Advance Interconnects and Contact Materials and Processes for Future Integrated Circuits*, ed. S. P. Murarka, D. B. Fraser, M. Eizenberg, R. Tung, R. Madar, Mater. Res. Soc. Proc. **514**, 75, Warrendale, PA (1998).
5. T. J. O'Keefe, Method for Stripping Metals in Solvent Extraction, U. S. Patent #5,228,903, July 20, 1993.
6. L. M. Chia, M. P. Niera, C. Flores, and T. J. O'Keefe in *Extraction and Processing for the Treatment and Minimization of Wastes*, ed. J. P. Hager et al, TMS Annual Meeting, 279, Warrendale, PA (1994).
7. M. J. O'Keefe, K. D. Leedy, J. T. Grant, M. Fang, H. Gu, and T. J. O'Keefe, *J. Vac. Sci. Tech. B* **17**(5), 2366 (1999).

## 5. Properties of Sputtered Bilayer $WN_x/W$ Diffusion Barriers between Si and Cu

K. D. Leedy, M. J. O'Keefe<sup>1</sup>, E. J. Dahlgren<sup>1</sup> and J. T. Grant<sup>2</sup>

Air Force Research Laboratory, Sensors Directorate, Wright-Patterson AFB, OH 45433

<sup>1</sup>University of Missouri-Rolla, Dept. of Metallurgical Engineering, Rolla, MO 65401

<sup>2</sup>Research Institute, University of Dayton, Dayton, OH 45469

### 5.1 Abstract

Copper interconnect metallizations in next generation integrated circuits will require thin diffusion barrier layers (<20 nm) between the Cu and low-k dielectric which may also function as seed layers for subsequent material depositions. One possible structure entails a multicomponent diffusion barrier with a lower resistivity component, such as W on  $WN_x$ . In this study, sputtered  $WN_x/W$  bilayer thin films were investigated as diffusion barriers between Si and Cu. The total thickness of the  $WN_x/W$  bilayer was fixed at 20 nm while the  $WN_x$  thickness was varied from 0 to 20 nm. After deposition of the barrier films, a 100 nm thick Cu film was sputtered over the top of the a-W and amorphous  $WN_x$  bi-layer. The as-deposited  $WN_x/W$  film stress was found to be strongly dependent on the relative amount of  $WN_x$  and W present and the addition of a Cu overlayer was found to mitigate the stress levels. The  $WN_x/W$  barriers remained stable after 650°C anneals and exhibited phase transformations to  $W_2N$ . Microstructural characterization using transmission electron microscopy and x-ray diffraction and chemical analysis by x-ray photoelectron spectroscopy of the films were used to identify the as-deposited and transformed phases.

### 5.2 Introduction

Several refractory metals and their nitrides are good candidate materials for Cu diffusion barriers in Si-based integrated circuits [1]. An optimal barrier layer should have a dense, amorphous microstructure, a smooth surface morphology, thermal stability with Cu and Si, low film stress and minimal thickness (10 to 20 nm) [2, 3]. Amorphous thin films are considered more effective diffusion barriers than polycrystalline thin films because of the lack of grain boundaries which function as fast diffusion paths [4]. Because of high temperature anneals used in the fabrication of semiconductor devices, the thermal stability of barrier films is an important consideration with respect to crystallinity and stress. W and  $WN_x$  have been studied individually as barrier layers, but their combination in thin bilayers is the subject of this study.

Tungsten nitride thin films have been shown to be stable at thicknesses less than 25 nm [5]. Fabrication methods for  $WN_x$  films include plasma enhanced chemical vapor deposition (PECVD) [6-10], reactive sputter deposition [11-16] and metal-organic chemical vapor deposition [17].

The intrinsic stress of  $WN_x$  thin films has been addressed in only limited studies. Yu [18] measured a compressive stress range of ~ 1.75 to 3 GPa in 300 nm thick sputter deposited  $WN_x$  films deposited at 5 mTorr with  $N_2$  partial flows from 0 to 40 %. Lee [6] studied stress relaxation in 300 nm thick PECVD  $WN_x/W$  bilayers by balancing W tensile stresses with  $WN_x$  compressive stresses. Shen [16] observed mostly compressive stresses in 150 nm thick  $WN_x$

films sputter deposited at 6 and 25 mTorr and noted a stress dependency on total gas pressure as well as nitrogen partial pressure.

Recent research has shown  $WN_x$  to be an effective barrier to Cu diffusion, with most studies using sputter deposition to fabricate the barrier films. Suh [11] observed a 100 nm amorphous  $WN_x$  barrier to be stable up to 800°C and a 5 nm barrier to be stable to 600°C. Uekubo [5] observed a 25 nm polycrystalline  $W_2N$  was required to maintain barrier properties up to 790°C and an 8 nm  $W_2N$  up to 600°C. Pokela [10] reported stable 120 nm thick  $WN_x$  barriers up to 750°C. Ganguli [13] reported good barrier performance in tungsten-rich, amorphous PECVD 15 nm  $WN_x$ . A 60 nm thick W barrier layer showed good barrier properties up to 600°C [9].

In this paper the influence of bilayer component film thicknesses on the properties and Cu barrier performance of reactive sputter deposited  $WN_x/W$  films was investigated.

### 5.3 Experiment

Tungsten and tungsten nitride thin films were deposited from a 99.95% pure W target using a Denton Vacuum Discovery 18 dc magnetron sputtering system with a base vacuum of  $1.4 \times 10^{-6}$  Pa. A mass flow regulated Ar- $N_2$  sputtering pressure of 0.53 Pa and 250 W forward power were held constant resulting in a nominal deposition rate of 0.3 nm/s. The  $N_2$  partial flow rate (the ratio of the nitrogen flow rate to the total flow rate of nitrogen and argon) was fixed at 30% to produce the tungsten nitride film. Tungsten films were deposited in a 0.53 Pa Ar atmosphere with 250 W forward power. The  $WN_x$  film was selected based on a previous investigation of  $WN_x$  films [15] as a function of nitrogen content. The  $WN_x$  film has approximately 29 at. % nitrogen and exhibited a predominantly amorphous structure up to 400°C. Si (100) wafers of 75 mm diameter and holey carbon support films on 3 mm grids were used as substrate materials during the study.  $WN_x$  was selected as the first layer primarily because W is known to react with Si to form  $W_5Si_3$  at approximately 600°C [5]. The total thickness of the  $WN_x/W$  bilayer was fixed at 20 nm while the  $WN_x$  thickness was varied from 0 to 20 nm. After deposition of the barrier films and without breaking vacuum, a 100 nm thick Cu film was sputter deposited over the  $WN_x/W$  bilayer. Cu films were deposited from a 99.99% pure Cu target in a 0.53 Pa Ar atmosphere with 250 W forward power. A water-cooled substrate holder was used without external heating for all of the depositions.

The intrinsic stress of the  $WN_x$  films was calculated using the wafer curvature technique and Stoney's equation. A laser reflectometry Flexus 2900 thin film stress system was used to measure the intrinsic stress of the as-deposited  $WN_x/W/Cu$  films on the Si substrates. Rapid thermal anneals of films were performed in an AG Associates Heatpulse 210 at 650°C for 15 min in flowing Ar-5% $H_2$  forming gas. X-ray diffraction (XRD) was done using a Rigaku D-MAX III thin film diffractometer with a fixed, low angle ( $5^\circ$ ) Cu  $K\alpha$  radiation source and a rotating sample holder. Morphology and crystal structure of  $WN_x/W/Cu$  films were examined by cross sectional transmission electron microscopy (TEM) using a Philips CM 200 at 200 kV. Film composition was determined with a Physical Electronics model 5700 Auger electron spectroscopy (AES) system. A 1mm x 1mm rastered 3 keV  $Ar^+$  ion beam was used to sputter through the  $Cu/W/WN_x$  film structures until the Si substrate was exposed, resulting in a crater. A 5 keV electron beam was then used to examine the composition at several points along the sloping crater wall, corresponding to different depths within the film structure, with AES [19].

## 5.4 Results

### Resistivity

Figure 5.4.1 shows the resistivity of 20 nm  $WN_x/W$  bilayer films. The individual  $WN_x$  film resistivity was  $158 \mu\Omega \text{ cm}$  and the W film was  $18 \mu\Omega \text{ cm}$ . Bilayer  $W/WN_x$  films displayed resistivities between these values, attributed to indentation of the four-point probe tips and preferential measurement of surface material resistivity. Anneals at  $650^\circ\text{C}$  yielded lower  $WN_x/W$  resistivities attributed to elimination of defects and phase transformation to polycrystalline  $W_2N$ . As deposited  $WN_x/W$  films with Cu overlayers had resistivities  $< 5 \mu\Omega \text{ cm}$ . Following  $650^\circ\text{C}$  anneals of  $Cu/W/WN_x/Si$  samples, the multilayer resistivities maintained  $< 5 \mu\Omega \text{ cm}$  except for the  $Cu/W/Si$  sample, which increased to  $89 \mu\Omega \text{ cm}$  due to the formation of  $Cu_3Si$ .

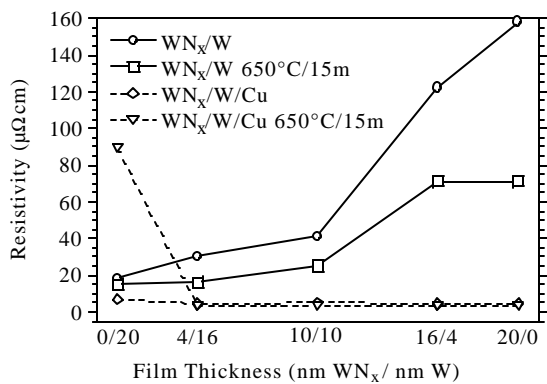


**Figure 5.4.1** Resistivity of  $WN_x/W$  and  $WN_x/W/Cu$  films, as-deposited and after  $650^\circ\text{C}$  anneals.

| Film<br>(nm $WN_x$ / nm W)<br>/ 100 nm Cu | As-<br>deposited | $650^\circ\text{C}/ 15$ min.<br>annealed |
|---|------------------|--|
| 0/20                                      | Cu, a-W          | a-W, $Cu_3Si$                            |
| 4/16                                      | Cu, a-W          | Cu, a-W                                  |
| 10/10                                     | Cu, a-W          | Cu, a-W, $W_2N$                          |
| 16/4                                      | Cu, a- $WN_x$    | Cu, $W_2N$ , a-W                         |
| 20/0                                      | Cu, a- $WN_x$    | Cu, $W_2N$ , a-W                         |

**Table 5.4.1** Crystal structure of  $WN_x/W/Cu$  films as-deposited and after  $650^\circ\text{C}$  anneal for 15 min. (a-  $WN_x$ , amorphous  $WN_x$ )

### XRD and TEM

Cu reflections with a (111) preferred orientation were observed in all as-deposited samples. Figure 5.4.2 shows x-ray diffraction scans from selected bilayer samples. The underlying diffusion barrier structure was evident as a-W in samples with  $> 10$  nm of W and amorphous  $WN_x$  in samples with 16 and 20 nm of  $WN_x$ . Reflections from W and  $WN_x$  component layers  $< 10$  nm thick were typically not visible in the x-ray scans. Table 5.4.1 shows the  $WN_x/W/Cu$  crystal structures observed in the as-deposited state and after  $650^\circ\text{C}$  anneals for 15 min. Following  $650^\circ\text{C}$  anneals, the W-only barrier was shown to be ineffective in stopping Cu diffusion as indicated by  $Cu_3Si$  formation. Cu reflections were observed in all samples except the W-only barrier as shown in Figure 5.4.3.  $WN_x/W$  bilayer and  $WN_x$ -only barriers showed no evidence of copper silicides or tungsten silicides. The amorphous  $WN_x$  transformed to  $W_2N$  in an amount proportional to the  $WN_x$  component. Some conversion of  $WN_x$  to  $\alpha$ -W due to annealing was also observed (studied extensively by Lin [7, 20]).

Cross sectional TEM analysis confirmed the stability of  $WN_x/W$  bilayers. Figure 5.4.4 shows the microstructure of a 4 nm  $WN_x$ / 16 nm W/ 100 nm Cu sample after a  $650^\circ\text{C}$  anneal. The barrier is continuous with no evidence of diffusion across the  $WN_x/W$  bilayer. A 2 nm thick reaction product is apparent at the  $WN_x/Si$  interface.  $W_5S_3$  was observed by XRD at a W/Si

interface after 650°C anneals in another study [5]. The interfacial phase in the current investigation is likely  $W_5Si_3$ , but insufficient amounts are present to appear in XRD scans.

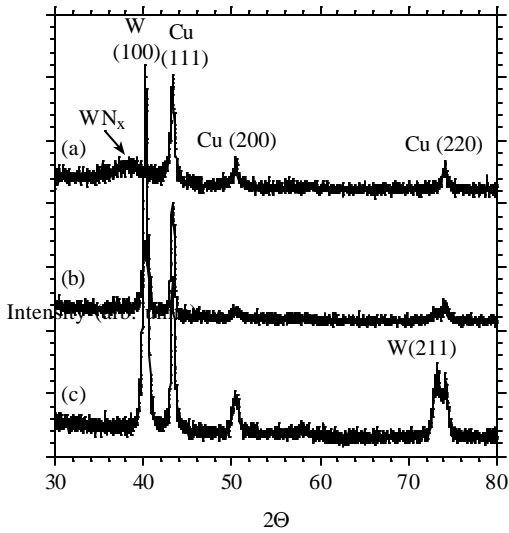


**Figure 5.4.2** X-ray diffraction profiles for selected as-deposited films: a) 20 nm  $WN_x$ /100 nm Cu, b) 10 nm  $WN_x$ /10 nm W/100 nm Cu and c) 20 nm W/100 nm Cu.

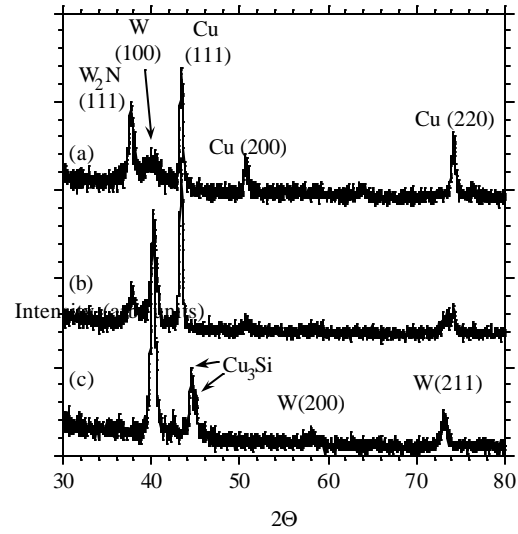


**Figure 5.4.3** X-ray diffraction profiles for selected 650°C annealed films: a) 20 nm  $WN_x$ /100 nm Cu, b) 10 nm  $WN_x$ /10 nm W/100 nm Cu and c) 20 nm W/100 nm Cu.

## AES

Two  $WN_x$ /W/Cu films annealed at 650°C were analyzed by taking AES measurements along part of the crater wall after sputtering with  $Ar^+$ . The films examined were 10 nm  $WN_x$ /10 nm W/100 nm Cu and 16 nm  $WN_x$ /4 nm W/100 nm Cu, and the results from 10 nm  $WN_x$ /10 nm W/100 nm Cu are shown in Figure 5.4.5. Figure 5.4.5(a) shows a scanning electron microscopy (SEM) image of a crater after sputtering through the Cu, W, and  $WN_x$  layers. The exposed Si substrate is the central, dark region. Auger spectra were acquired at several points along the crater wall, and those acquired at points marked 1, 2, 3, and 4 in the SEM image are plotted in Figure 5.4.5(b). Scan 1, taken near the inner edge of the crater wall, shows mainly Si with a smaller amount of W (the main, high energy Si and W peaks have similar sensitivity factors). No Cu was detected at point 1 (the Cu detection limit for conditions used here was less than 1 atomic %). Points 2 and 3 were taken further up the crater wall and show increasing W. Note the presence of Cu (about 5 atomic %) at point 3. Point 4 was taken on the sputtered Cu. Similar results were obtained from the other sample. These AES results confirm the XRD results showing the effectiveness of the  $WN_x$ /W in preventing Cu diffusion into the Si.

## Stress

The as-deposited average film stress in  $WN_x$ /W bilayer films (Figure 5.4.6) was tensile in films without  $WN_x$  and became compressive with increasing  $WN_x$  thickness component. A substantial 4 GPa range in film stress was measured in the studied  $WN_x$ /W films. Compressive stresses in  $WN_x$  are generated by N atom incorporation in the W lattice that collapses into an amorphous structure. The tensile W stresses and compressive  $WN_x$  stresses are consistent with another investigation [6].



$WN_x/W$  bilayer films with a sputter deposited 100 nm Cu overlayer displayed a notable moderation in stress, tensile and compressive. For comparison, the stress of a 100 nm Cu film was 150 MPa. One possibility for the reduction in stress may be the domination of the thicker Cu over the thinner  $WN_x/W$  layer. Also, Flexus calculations are more accurate for thicker films. Anneals at 650°C generated a 800 MPa tensile stress increase in  $WN_x/W/Cu$  films attributed to tungsten nitride phase transformations, annihilation of defects, and grain growth. An exception to the post-anneal tensile stress increase occurred in the W/Cu film due to  $Cu_3Si$  formation.

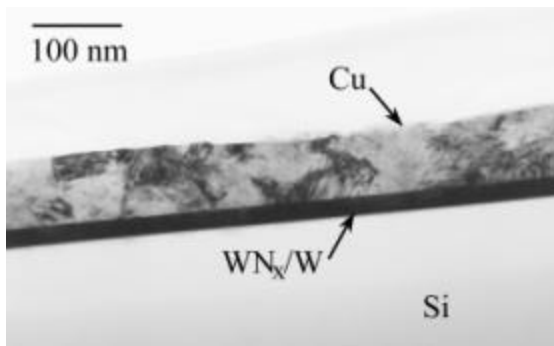
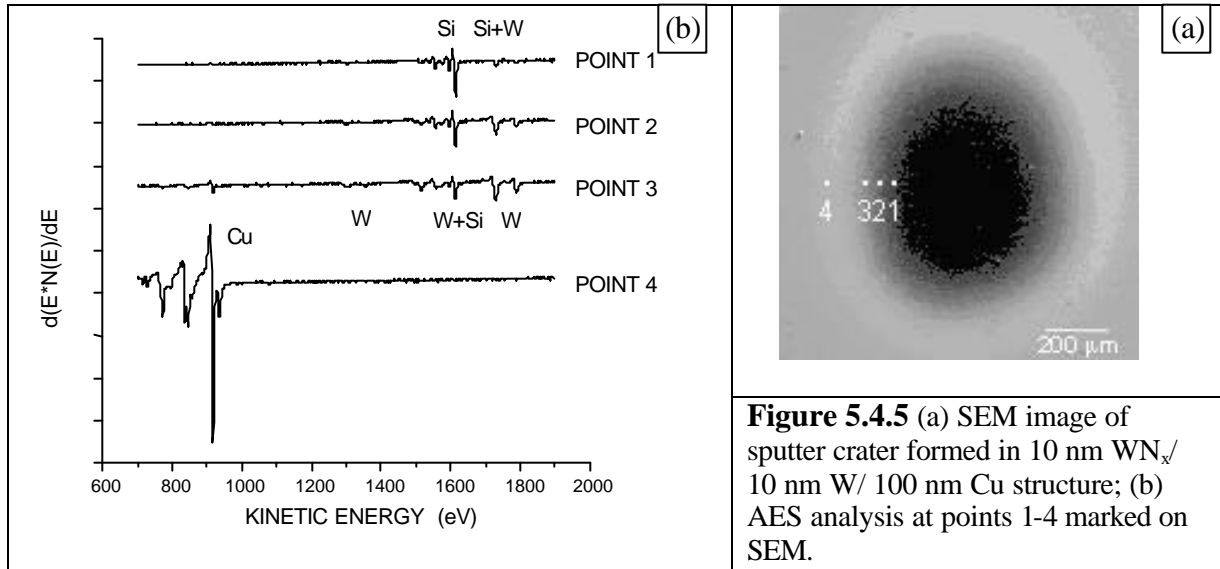


**Figure 5.4.4** Cross sectional TEM image of 650°C annealed 4 nm  $WN_x$ /16 nm W/ 100 nm Cu.

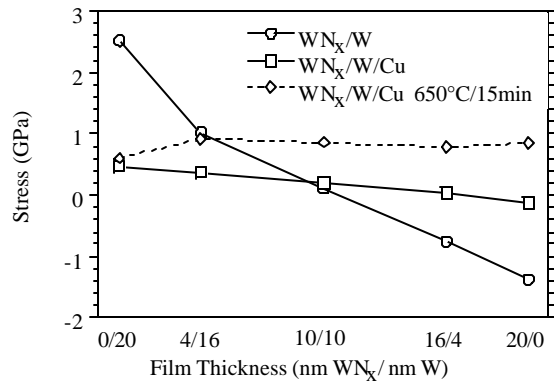


**Figure 5.4.6** Average stress of  $WN_x/W$  and  $WN_x/W/Cu$  films, as-deposited and after 650°C anneals.

## 5.5 Conclusions

Bilayer  $WN_x/W$  thin films were found to be stable diffusion barriers at the annealing temperature of 650°C as determined by X-ray diffraction, AES measurements and cross sectional TEM. Resistivities of the bilayer  $WN_x/W$  thin films were between that of W (18  $\mu\Omega/\text{cm}$ ) and  $WN_x$  (158  $\mu\Omega/\text{cm}$ ) component films. Anneals at 650°C caused the amorphous  $WN_x$  component to transform to  $W_2N$  and a-W. Individual W film stress was highly tensile and  $WN_x$  exhibited high compressive stress while the stress of bilayer  $WN_x/W$  films fell in between. The addition of a Cu overlayer film helped mitigate the tensile and compressive  $WN_x/W/Cu$  stresses while post deposition anneals of the samples resulted in a tensile stress increase.

## Acknowledgments

The authors gratefully acknowledge J. Boeckl for TEM sample preparation and support provided by the Materials and Manufacturing Directorate (J.T.G.). Partial support was provided by the University of Missouri Research Board and the U.S. Department of Education under the GAANN program.

## 5.6 References

1. C. Galewski and T. Seidel, European Semiconductor Design Production Assembly **21(1)**, 31 (1999).
2. S. S. Wong, C. Ryu, H. Lee and K.-W. Kwon in *Advanced Interconnects and Contact Materials and Processes for Future Integrated Circuits*, edited by S. P. Murarka, D. B. Fraser, M. Eizenberg, R. Tung, R. Madar (Mater. Res. Soc. Proc. **514**, Warrendale, PA, 1998) pp. 75-81.
3. B. Chin et al., Solid State Technol. **41(7)**, 141 (1998).
4. X. Sun, E. Kolawa, J.-S. Chen, J. S. Reid and M.-A. Nicolet, Thin Solid Films **236**, 347 (1993).
5. M. Uekubo, T. Oku, K. Nii, M. Murakami, K. Takahiro, S. Yamaguchi, T. Nakano and T. Ohta, Thin Solid Films **286**, 170 (1996).
6. C. W. Lee and Y. T. Kim, Appl. Phys. Lett. **65(8)**, 965 (1994).
7. J. Lin, A. Tsukune, T. Suzuki and M. Yamada, J. Vac. Sci. Technol. A **17(3)**, 936 (1999).
8. C. W. Lee, Y. T. Kim, C. Lee, J. Y. Lee, S.-K. Min and Y. W. Park, J. Vac. Sci. Technol. B **12(1)**, 69 (1994).
9. H. Ono, T. Nakano and T. Ohta, Appl. Phys. Lett. **64(12)**, 1511 (1994).
10. P. J. Pokela, C.-K. Kwok, E. Kowala, S. Raud and M.-A. Nicolet, Appl. Surface Science **53**, 364 (1991).
11. B.-S. Suh, Y.-J. Lee, J.-S. Hwang and C.-O. Park, Thin Solid Films **348**, 299 (1999).
12. F. C. T. So, E. Kolawa, X.-A. Zhao, E. T.-S. Pan and M.-A. Nicolet, J. Appl. Phys. **64(5)**, 2787 (1988).
13. S. Ganguli, L. Chen, T. Levine, B. Zheng and M. Chang, J. Vac. Sci. Technol. B **18(1)**, 237 (2000).
14. H. Yongjun, U. S. Patent No. 5633200, 1997.
15. K. D. Leedy, M. J. O'Keefe, J. G. Wilson, R. Osterday, and J. T. Grant in *Materials, Technology and Reliability for Advanced Interconnects and Low-k Dielectrics*, edited by K.

- Maex, Y-C. Joo, G.S. Oehrlein, S. Ogawa and J.T. Wetzel (Mater. Res. Soc. Proc. **612**, Warrendale, PA, 2001) in press.
16. Y. G. Shen and Y. W. Mai, Surface and Coatings Technol. **127**, 239 (2000).
  17. J. E. Kelsey, C. Goldberg, G. Nuesca, G. Peterson and A. E. Kaloyeros, J. Vac. Sci. Technol. B **17(3)**, 1101 (1999).
  18. K. M. Yu, J. M. Jaklevic, E. E. Haller, S. K. Cheung and S. P. Kwok, J. Appl. Phys. **64(3)**, 1284 (1988).
  19. J. T. Grant in *Methods in Materials Research*, edited by E.N. Kaufmann, (John Wiley & Sons), 11d.2, pp.1-19 (2000).
  20. J. Lin, A. Tsukune, T. Suzuki and M. Yamada, J. Vac. Sci. Technol. A **16(2)**, 611 (1998).